DNA Assembly of Dye Aggregates—A Possible Path to Quantum Computing

Bernard Yurke

Abstract DNA-based self-assembly enables the programmable arrangement of matter on a molecular scale. It holds promise as a means with which to fabricate high technology products. DNA-based self-assembly has been used to arrange chromophores (dye molecules) covalently linked to DNA to form Förster resonant energy transfer and exciton-based devices. Here we explore the possibility of making coherent exciton information processing devices, including quantum computers. The focus will be on describing the chromophore arrangements needed to implement a complete set of gates that would enable universal quantum computation.

1 Introduction

Already in the earliest days of DNA nanotechnology, Richardson and Seeman imagined using DNA nanotechnology to fabricate electronic information storage and processing devices, such as three-dimensional memories in which the wires and switching elements were of molecular scale [1]. My own entry into this field, in the late 1990s, at Bell Laboratories, was motivated by this vision. The tools of DNA nanotechnology have undergone considerable development since those early days [2, 3], but its use in the construction of electronic or photonic information processing systems is still in its infancy. One of the more developed areas is the use of DNA nanotechnology to arrange metallic nanoparticles, quantum dots and dyes in desired configurations [4–9], (here referred to as aggregates) aimed at making photonic devices. A recent development is the use of DNA self-assembly to construct dye aggregates in which the distance between the dyes is sufficiently close that excited-state energy can be transferred between neighboring dyes in a manner that maintains quantum coherence [10–17]. The packet of energy that is transferred between dyes is referred to as an exciton and that exhibits quantum mechanical particle-like properties. The possibility of using such aggregates as quantum gates

B. Yurke (✉)
Micron School of Materials Science & Engineering and Department of Electrical and Computer Engineering, Boise State University, Boise, ID 83725, USA
e-mail: bernardyurke@boisestate.edu

N. Jonoska and E. Winfree (eds.), *Visions of DNA Nanotechnology at 40 for the Next 40*, Natural Computing Series, https://doi.org/10.1007/978-981-19-9891-1_9

and quantum computers was raised by Castellanos et al. [18, 19]. They exhibited dye aggregate configurations that implemented the function of a set of three types of gates that would enable universal quantum computation. As the authors point out, however, their embodiment of these gates does not allow one to exploit the full power of quantum computation. To to accomplish that, the authors note, use must be made of the interaction between two excitons. Here a set of gates is provided for which the interaction between two excitons is employed in the implementation of the controlled not (CNOT) gate. These gates do form a complete set enabling universal quantum computation. The quantum computation scheme employed is that of a many particle quantum walk, similar to the scheme proposed by Childs et al. [20]; however, here a dual-rail architecture is employed that greatly simplifies gate design.

Random perturbations of excitons by molecular vibrations tend to wash out the delicate quantum interference effects on which quantum computing relies. Other would-be quantum computing technologies also must contend with random processes by which quantum interference effects are washed out. This problem, however, is sufficiently severe for exciton-based quantum gates that it poses a significant challenge to exciton-based quantum computation's capacity to win the race against all the other quantum computation technologies being developed [21–23]. Whether dyes can be synthesized for which the interaction between excitons and molecular vibrations is sufficiently weak to enable more than the demonstration of rudimentary quantum computing circuits remains to be seen. The employment of devices based on molecular transitions at the energy scale of visible light photons does open, however, the prospect for quantum gate operation at room temperature and with femtosecond switching speeds. Quantum computation through the assembly of dye aggregates via DNA-based self-assembly thus provides a reach goal to drive the development of high technology photonic devices in which the gates are of molecular scale, have high switching speeds, and the circuits have high component density.

Although the scope here is limited to dye aggregate architectures that can function as exciton-based quantum gates for universal quantum computation, with the implicit understanding that currently DNA self-assembly is the most promising means by which to assemble such aggregates, it worth noting that the study excitons in dye aggregates and molecular crystals has a long and extensive history [24]. This history predates the field of DNA assembly, beginning with theoretical work by Frenkel [25] in 1931 and the experimental work by Jelley [26] in 1936 and by Scheibe et al. [27–29] in 1937.

As indicated, here we explore the possibility of making information processing devices out of dye aggregates constructed by DNA self-assembly. Dye molecules exhibit color due to their ability to absorb light at specific wavelengths. The process occurs because the molecule has a transition from the ground state to an excited state that can be induced by the absorption of a visible light photon. Such a transition is said to be optically allowed in order to distinguish it from transitions that require a change in the total electron spin angular momentum, something that the absorption of a photon alone cannot do, or transitions that a photon cannot induce for symmetry or other reasons.

The bundle of energy stored in the molecule upon absorption of a photon can be transferred from one dye molecule to a neighboring dye molecule. In this process one dye molecule returns to its ground state while simultaneously the other is promoted from its ground state to its optically allowed excited state. This bundle of energy that once was a photon can thus propagate from dye molecule to dye molecule throughout an aggregate of dye molecules. In this manner the bundle of energy behaves like a particle and could be used as a carrier of information much like an electron.

This bundle of energy, which resides on one dye molecule at a time, is referred to as an exciton. Technically, this bundle of energy is referred to as a Frenkel exciton to distinguish it from a Wannier–Mott exciton which is an electron–hole pair residing in a semiconductor material. Either is simply referred to as an exciton, when it is clear from context which type of exciton is meant.

When the spacing between dyes becomes 2 nm or less, the hopping occurs in a coherent manner, which enables the exciton to behave like a quantum mechanical particle exhibiting wave-like behavior. This is where quantum mechanical wave-particle duality enters. Even though at any instant of time the exciton resides on only one dye, the exciton behaves as if it is a wave spread out over the entire dye aggregate.

When a pair of neighboring dyes are both in their excited state, the electrostatic energy between the dyes will be different from that when only one dye is excited due to the change in a dye's electron density distribution that occurs when the dye transitions from the ground state to the excited state. This gives rise to a two-body or exciton–exciton interaction in which excitons scatter off of each other.

These two properties, the ability of an exciton to coherently hop from dye to dye and the ability of two excitons to scatter off of each other, in principle, enable suitably structured dye aggregates to function as quantum gates, information processing systems and maybe even as quantum computers.

In the following sections a set of dye configurations will be described that form a complete set of gates for universal quantum computation. Also described is how these gates can be assembled into functioning information processing systems and quantum computers. Nonidealities that must be overcome to realize such devices are also discussed.

2 The Mathematical Structure of Reality

Here a brief introduction to quantum mechanics is provided with the aim to give some indication of where the power of quantum computing resides. Quantum theory has survived 100 years of rigorous testing and, as near as can be discerned, provides the foundational description of all physical phenomena. This includes physical computation processes. In this sense all computers are quantum computers. But not all computers take advantage of the additional computing resources that quantum mechanics provides beyond those utilized by computers relying on classical physics.

As an indication of how reality, by which we mean the state of a physical system, is represented in quantum mechanics, consider first a classical mechanical system.

At any given instant of time, such a system will possess a number of attributes that can be measured such as its position, its momentum, angular momentum and energy. The list of numbers needed to specify the state of the system can be shorter than the complete list of attributes. For example, for a point particle the energy and angular momentum can be computed if the position and momentum are known. Thus, the particle's position and momentum provide a complete specification of its state. In contrast to classical systems, in which the attributes can take on any real number value, in quantum mechanical systems, a measurement of an attribute often will only yield one of a discrete list of values: that is, the attribute is quantized. For example, for an electron in a hydrogen atom, the total angular momentum J and the z-component of the total angular momentum J_z, if measured, take on the discrete values $\hbar\sqrt{j(j+1)}$ and $\hbar m_j$, respectively, where $\hbar$ is Planck's constant, j is a half integer greater than zero, that is, $j \in \{1/2,\ 3/2,\ 5/2, \ldots\}$, and m_j is a half integer in the range $-j \le m_j \le j$. Given j and m_j, the energy of the electron can be computed. Indeed, j and m_j provide a complete specification of the state of the electron for which j and m_j have been measured and this state is often denoted by $|j, m_j\rangle$. Such states, however, do not exhaust the states that the electron can be in. The electron can be in any state $|\psi\rangle$ of the form

$$|\psi\rangle = \sum_{j=1/2}^{\infty} \sum_{m_j=-j}^{j} \alpha_{j,m_j} |j, m_j\rangle. \tag{1}$$

where the $\alpha_{j.m}$ are complex numbers subject to the constraint

$$\sum_{j=1/2}^{\infty} \sum_{m_j=-j}^{j} |\alpha_{j,m_j}|^2 = 1. \tag{2}$$

Note that the state $|\psi\rangle$ can be represented as a column vector listing all the α_{j,m_j}:

$$|\psi\rangle = \begin{bmatrix} \alpha_{1/2,-1/2} \\ \alpha_{1/2.1/2} \\ \alpha_{3/2,-3/2} \\ \alpha_{3/2,-1/2} \\ \alpha_{3/2,1/2} \\ \alpha_{3/2,3/2} \\ \cdot \\ \cdot \\ \cdot \end{bmatrix}. \tag{3}$$

If one performs a measurement of J and J_z on this state, the probability of obtaining the quantum numbers j and m_j from the measurement is $|\alpha_{j,m_j}|^2$. The measurement of J and J_z must yield some value for j and m_j. Hence, Eq. (2) is simply the statement that the sum of the probabilities of measurement outcomes over all

possible measurement outcomes must be 1. It is tempting to interpret $|\psi\rangle$ of Eq. (1) as representing a statistical ensemble for which $|\alpha_{j,m_j}|^2$ is the fraction of systems in the state $|j, m_j\rangle$; however, with more than one nonzero α_{j,m_j}, states having the from Eq. (1) can give rise to observable interference effects if the x-component J_x or y-component J_y of the angular momentum is measured, thereby making an ensemble interpretation untenable.

Having introduced quantum mechanical state vectors via the example of an electron in a hydrogen atom, the discussion will now proceed on a more general and abstract level. The state $|\psi\rangle$ of a quantum mechanical system consists of an N-dimensional vector where N could be ∞. The state can be represented by a column vector

$$|\psi\rangle = \begin{bmatrix} \alpha_1 \\ \alpha_2 \\ \cdot \\ \cdot \\ \cdot \\ \alpha_N \end{bmatrix} \tag{4}$$

where the α_i are complex functions of time. The Hermitian adjoint (the matrix that results when one interchanges rows and columns of a matrix and takes the complex conjugate of the matrix elements) of $|\psi\rangle$ is given by

$$\langle\psi| = [\alpha_1^* \; \alpha_2^* \; \cdot \; \cdot \; \cdot \; \alpha_N^*]. \tag{5}$$

To provide quantum mechanics with a probability interpretation, a norm of the state vector $|\psi\rangle$ is introduced and denoted by $\langle\psi|\psi\rangle$ and defined by the matrix product

$$\langle\psi|\psi\rangle \equiv \left[\alpha_1^* \; \alpha_2^* \; \cdot \; \cdot \; \cdot \; \alpha_N^*\right] \begin{bmatrix} \alpha_1 \\ \alpha_2 \\ \cdot \\ \cdot \\ \cdot \\ \alpha_N \end{bmatrix} = \sum_{m=1}^{N} |\alpha_m|^2. \tag{6}$$

The probability interpretation is imposed by requiring the state vector to have unit norm $\langle\psi|\psi\rangle = 1$. Then $|\alpha_m|^2$ is the probability of finding the system in the state represented by the mth position of the state vector.

The dynamics of a quantum mechanical system is governed by the Schödinger equation

$$i\hbar\frac{\partial}{\partial t}|\psi\rangle = H|\psi\rangle, \tag{7}$$

where t is the time and H is the Hamiltonian. The Hamiltonian is an $N \times N$ array. The values for the elements of this array depend on the system under consideration and are ultimately determined by experiment, though procedures, such as canoni-

cal quantization, are available that enable one to generate the Hamiltonian from a classical mechanical description of the system. The Hamiltonian is required to be Hermitian, that is, if the rows and columns are interchanged and the complex conjugate of all the matrix elements is taken, one winds up with the same matrix. This ensures that the Hamiltonian only has real eigenvalues, which turn out to be the energy eigenvalues of the system.

Equation (7) can be formally integrated to yield

$$|\psi(t)\rangle = U(t, t_0)|\psi(t_0)\rangle \tag{8}$$

where

$$U(t, t_0) = \exp\left(-\frac{i}{\hbar}\int_{t_0}^{t} H\mathrm{d}t\right). \tag{9}$$

Since H is Hermitian, the Hermitian conjugate of $U(t, t_0)$ is

$$U^{\dagger}(t, t_0) = \exp\left(\frac{i}{\hbar}\int_{t_0}^{t} H\mathrm{d}t\right). \tag{10}$$

It then follows that $U^{\dagger}(t, t_0)$ is unitary, that is

$$U^{\dagger}(t, t_0)U(t, t_0) = U(t, t_0)U(t, t_0)^{\dagger} = 1. \tag{11}$$

Thus, governed by the Schrödinger equation a system undergoes unitary time evolution. An important consequence of this is that the norm of $|\psi\rangle$ does not change with time, that is, probability is conserved in the sense that the sum of the probabilities of outcomes over all possible outcomes is 1, as required for a consistent probabilistic interpretation.

3 Quantum Computers

Having outlined the mathematical structure of reality, an indication is now provided of how the power of quantum computation arises. Apart from unitarity, quantum mechanics places no further restrictions on the unitary transformations that can be physically realized. Of course, the challenge is to find or engineer physical systems that can perform the unitary transformations that carry out the desired computation. Here we take for granted that for any desired unitary transformation a physical system can be engineered that carries out that unitary transformation.

It is convenient to introduce some further notation. The state vector Eq. (4) can be written as

$$|\psi\rangle = \sum_{m=1}^{N} \alpha_m |m\rangle, \tag{12}$$

where the $|m\rangle$ are time-independent unit basis vectors satisfying the orthonormality condition

$$\langle m|m'\rangle = \delta_{m,m'} \tag{13}$$

where $\delta_{m,m'}$ is the Kronecker delta function. The Kronecker delta function is zero when $m \neq m'$ and one when $m = m'$.

Consider now a two-state system where one basis state has been arbitrarily chosen to represent a logical 0, whereas the orthogonal basis state is chosen to represent a logical 1. Denoting these states by $|0\rangle$ and $|1\rangle$, respectively, an arbitrary state of the system is then given by

$$|\psi\rangle = \alpha_0|0\rangle + \alpha_1|1\rangle = \begin{bmatrix} \alpha_0 \\ \alpha_1 \end{bmatrix}. \tag{14}$$

This $|\psi\rangle$ could be the state of a binary memory register. A classical binary memory register can be in only one of two mutually exclusive states, a logical 0 or a logical 1. In contrast, a quantum mechanical binary memory register can be in any state of the form of Eq. (14). In the general case, the contents of the binary memory register must be specified by two complex numbers, α_0 and α_1 with the restriction $|\alpha_0|^2 + |\alpha_1|^2 = 1$. Although $|\alpha_0|^2$ and $|\alpha_1|^2$ are the probabilities of finding the register content to be a logical 0 or a logical 1 if one looks at the contents, this does not represent a statistical mixture in which the memory register is in one state or the other. Otherwise a single number, $|\alpha_0|^2$, would be sufficient to describe the state of the system rather than two complex numbers with a constraint on the sum of their norms. The information encoded by the state Eq. (14) is referred to as a qubit. Its logical value is specified by the complex numbers α_1 and α_2.

A general unitary transformation of the state Eq. (14) has the form

$$\begin{bmatrix} \beta_0 \\ \beta_1 \end{bmatrix} = U \begin{bmatrix} \alpha_0 \\ \alpha_1 \end{bmatrix} \tag{15}$$

where

$$U = \begin{bmatrix} u_{11} & u_{12} \\ u_{21} & u_{22} \end{bmatrix}. \tag{16}$$

In general, the $u_{m,n}$ are complex numbers subject to the constraint that U be unitary, that is, $U^\dagger U = UU^\dagger = 1$. Here a quantum mechanical logic gate performing such a transformation is referred to as a basis change gate. Note that this gate is a one input and one output gate and consequently could be regarded as a generalization of a classical NOT gate. A special case of the basis change gate is the Hadamard gate, which is given by

$$U_H = \frac{1}{\sqrt{2}} \begin{bmatrix} 1 & 1 \\ 1 & -1 \end{bmatrix}. \tag{17}$$

This gate frequently shows up in quantum computing circuits. Suppose that initially the memory register is in the logical 0 state $|0\rangle$, then, subjected to a physical system that transforms the memory contents according to Eq. (17), the final state of the memory register will be $|\psi\rangle = (1/\sqrt{2})(|0\rangle + |1\rangle)$. A basis change gate thus provides a means for putting a memory element into a superposition state when initially it is in the logical 0 or logical 1 state. Another special case of the one input gate Eq. (15) is the phase gate:

$$U_P = \begin{bmatrix} e^{i\phi_0} & 0 \\ 0 & e^{i\phi_1} \end{bmatrix}. \tag{18}$$

This gate transforms the phases of the elements of a superposition state. For example, if the initial state of the memory element is given by $|\psi(t_0)\rangle = (1/\sqrt{2})(|0\rangle + |1\rangle)$, a physical system performing the operation Eq. (15) on the memory element will put it in the state $|\psi(t_1)\rangle = (1/\sqrt{2})(e^{i\phi_0}|0\rangle + e^{i\phi_1}|1\rangle)$.

3.1 The Controlled NOT Gate

It is noted that the phenomenon of classical wave interference is sufficient to realize any unitary transformation. For example, any unitary transformation on an N dimensional vector can be realized by an array of $N(N-1)/2$ optical beam splitters [30]. However, for certain unitary transformations, quantum mechanics provides a means to greatly reduce the number of parts needed to implement the unitary transformation. To indicate how this works the controlled not (CNOT) gate will now be considered.

The CNOT gate is a two-input two-output gate that is a generalization of a classical exclusive or (XOR) operation. Since this is a two-input gate, two interacting two-level systems are required to implement the gate, the control system and the target system. Let the Boolean bases states of the control system be denoted by $|0\rangle_C$ and $|1\rangle_C$ and the Boolean bases states of the target system be denoted by $|0\rangle_T$ and $|1\rangle_T$. The state space for the complete system is the outer product of the state space for the two subsystems. Hence, the basis states for the complete system can be written as

$$\begin{aligned} |1\rangle &= |0\rangle_C|0\rangle_T = |0,0\rangle \\ |2\rangle &= |0\rangle_C|1\rangle_T = |1,0\rangle \\ |3\rangle &= |1\rangle_C|0\rangle_T = |0,1\rangle \\ |4\rangle &= |1\rangle_C|1\rangle_T = |1,1\rangle. \end{aligned} \tag{19}$$

In the rightmost equalities the states have been written in the form $|x, y\rangle$ where x is the Boolean value of the control basis state and y is the Boolean value of the target basis state. In this basis, the unitary transformation performed by the CNOT gate has the matrix representation

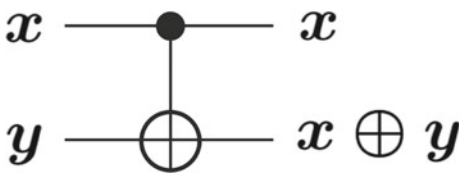

Fig. 1 Symbol for a CNOT gate. The input and output line labeled x is the control line. The target input is y. The target output is the XOR of x and y

$$U_{\text{CNOT}} = \begin{bmatrix} 1\,0\,0\,0 \\ 0\,1\,0\,0 \\ 0\,0\,0\,1 \\ 0\,0\,1\,0 \end{bmatrix}. \tag{20}$$

On the Boolean basis states this CNOT operation performs the following transformations:

$$\begin{aligned} |0,0\rangle &\rightarrow |0,0\rangle \\ |0,1\rangle &\rightarrow |0,1\rangle \\ |1,0\rangle &\rightarrow |1,1\rangle \\ |1,1\rangle &\rightarrow |1,0\rangle \end{aligned} \tag{21}$$

From this it is apparent that the control state x remains unchanged, whereas the target state y is transformed to $x \oplus y$, the XOR operation. The symbol for a CNOT gate in quantum computer diagrams is given in Fig. 1.

In general, the initial state of our two two-state system has the form

$$|\psi(t_0)\rangle = \begin{bmatrix} \alpha_{0,0} \\ \alpha_{0,1} \\ \alpha_{1,0} \\ \alpha_{1,1} \end{bmatrix} = \alpha_{0,0}|0,0\rangle + \alpha_{0,1}|0,1\rangle + \alpha_{1,0}|1,0\rangle + \alpha_{1,1}|1,1\rangle, \tag{22}$$

where the state vector has been written in two different forms, that of a column vector and that in which basis vectors in ket notation are employed. The result of operation of the CNOT gate on this state is obtained by multiplying the column vector form of the state by the matrix Eq. (20) representing the unitary transformation performed by the CNOT gate, as Eq. (15) indicates. The resulting state is

$$\begin{aligned} |\psi(t_1)\rangle &= \begin{bmatrix} 1\,0\,0\,0 \\ 0\,1\,0\,0 \\ 0\,0\,0\,1 \\ 0\,0\,1\,0 \end{bmatrix} \begin{bmatrix} \alpha_{0,0} \\ \alpha_{0,1} \\ \alpha_{1,0} \\ \alpha_{1,1} \end{bmatrix} = \begin{bmatrix} \alpha_{0,0} \\ \alpha_{0,1} \\ \alpha_{1,1} \\ \alpha_{1,0} \end{bmatrix} \\ &= \alpha_{0,0}|0,0\rangle + \alpha_{0,1}|0,1\rangle + \alpha_{1,0}|1,1\rangle + \alpha_{1,1}|1,0\rangle. \end{aligned} \tag{23}$$

Comparing these last two equations one sees that the CNOT gate simultaneously performs the correct logical operation on each Boolean component of the input state. This is an example of quantum parallelism.

3.2 *Quantum Parallelism*

To generalize the discussion of CNOT gate operation, consider the case of a memory register consisting of N two-state systems. For a classical memory register, each bit element is either in a logical 0 or logical 1 state. As a consequence, the register can store only one N bit binary number at a time. Quantum mechanically the register can be in any state of the form

$$|\psi(t_0)\rangle = \sum_{m_1=0}^{1} \sum_{m_2=0}^{1} \cdots \sum_{m_N=0}^{1} \alpha_{m_1,m_2,\ldots,m_N} |m_1, m_2, \ldots, m_N\rangle, \tag{24}$$

where, as indicated by the subscripts and superscripts of the sums, $m_i \in \{0, 1\}$. Each state label $m_1, m_2, \ldots, m_N$ is, thus, a binary number and the sum is over all possible N bit binary numbers. Equation (24) is a generalization of Eq. (22). Thus, a quantum mechanical memory register consisting of N two-level systems behaves as if it is simultaneously storing 2^N complex numbers subject to the constraint that the sum of the norm-squares of these complex numbers is 1. Singling out memory elements i and a j for operation on by a CNOT gate, Eq. (24) can be written as

$$\begin{aligned}
|\psi(t_0)\rangle = & \sum_{\{m_n | n \notin \{i,j\}\}} \alpha_{m_1,m_2,\ldots 0_i \ldots 0_j \ldots m_N} |m_1, m_2, \ldots 0_i \ldots 0_j \ldots m_N\rangle \\
& + \sum_{\{m_n | n \notin \{i,j\}\}} \alpha_{m_1,m_2,\ldots 0_i \ldots 1_j \ldots m_N} |m_1, m_2, \ldots 0_i \ldots 1_j \ldots m_N\rangle \\
& + \sum_{\{m_n | n \notin \{i,j\}\}} \alpha_{m_1,m_2,\ldots 1_i \ldots 0_j \ldots m_N} |m_1, m_2, \ldots 1_i \ldots 0_j \ldots m_N\rangle \\
& + \sum_{\{m_n | n \notin \{i,j\}\}} \alpha_{m_1,m_2,\ldots 1_i \ldots 1_j \ldots m_N} |m_1, m_2, \ldots 1_i \ldots 1_j \ldots m_N\rangle,
\end{aligned} \tag{25}$$

where the subscript on the sums indicates summation over all m_n as in Eq. (24), excluding the sum over m_i and m_j. Upon operation by the CNOT gate, the contents of the memory register, where i is the control qubit and j is the target qubit, are changed to

$$
\begin{aligned}
|\psi(t_1)\rangle = & \sum_{\{m_n|n\notin\{i,j\}\}} \alpha_{m_1,m_2,\ldots 0_i \ldots 0_j \ldots m_N} |m_1, m_2, \ldots 0_i \ldots 0_j \ldots m_N\rangle \\
& + \sum_{\{m_n|n\notin\{i,j\}\}} \alpha_{m_1,m_2,\ldots 0_i \ldots 1_j \ldots m_N} |m_1, m_2, \ldots 0_i \ldots 1_j \ldots m_N\rangle \\
& + \sum_{\{m_n|n\notin\{i,j\}\}} \alpha_{m_1,m_2,\ldots 1_i \ldots 1_j \ldots m_N} |m_1, m_2, \ldots 1_i \ldots 1_j \ldots m_N\rangle \\
& + \sum_{\{m_n|n\notin\{i,j\}\}} \alpha_{m_1,m_2,\ldots 1_i \ldots 1_j \ldots m_N} |m_1, m_2, \ldots 1_i \ldots 0_j \ldots m_N\rangle .
\end{aligned}
\tag{26}
$$

This equation is a generalization of Eq. (23). Thus, the CNOT gate simultaneously performs the correct Boolean operation on each of the 2^N Boolean basis states of the superposition.

Not all computations can take advantage of this quantum parallelism. The identification of computational tasks of practical interest that can benefit from quantum speedup has been slow in coming but include important problems such as factoring large numbers and doing database searches. The quantum computing algorithms for these two problems were discovered by Shor [31] and Grover [32] respectively.

The CNOT gate, the Hadamard gate, together with the phase gates, form a complete set of gates for universal quantum computation [33]. Thus, this set of gates plays a role similar to that of the NAND gate of classical electronic circuit design, the gate with which any Boolean function can be implemented.

4 The Frenkel Exciton Hamiltonian

Having displayed a complete set of gates that enable universal quantum computation, we now work toward showing how these gates might be realized by dye aggregates. To this end, a Hamiltonian governing the dynamics of excitons is now introduced, the Frenkel exciton Hamiltonian. This is a phenomenological or reduced Hamiltonian, in that it contains parameters that must be determined by experiment or by calculation methods, such as time-dependent density functional theory, that are closer to first principles calculations. Here interaction of excitons with molecular vibrations is neglected. How these may be included is discussed in Sect. 16.

The Frenkel exciton Hamiltonian is given by Abramavicius et al. [34], Renger et al. [35]

$$
\begin{aligned}
H = & \sum_{m=1}^{N} E_m^e B_m^\dagger B_m + \sum_{(m,n)} J_{(m,n)} (B_m^\dagger B_n + B_n^\dagger B_m) \\
& + \frac{1}{2} \sum_{m=1}^{N} \Delta_m B_m^\dagger B_m^\dagger B_m B_m + \sum_{(m,n)} K_{(m,n)} B_m^\dagger B_n^\dagger B_n B_m .
\end{aligned}
\tag{27}
$$

Here the summation index (m, n) denotes summation over all distinct pairs dye molecules, and N is the total number of dyes in the aggregate.

E_m^e is the transition energy from the ground state to the first optically allowed excited state of molecule m. $J_{(m,n)}$ is the exciton exchange energy, which arises from the Coulomb interaction between the transition charge densities [34] of dye pair m and n. Δ_m is the anharmonicity parameter [35] that quantifies the energy cost with having two excitons occupy the same dye. It can be understood as follows. Let S_0 denote the ground state of the dye. The lowest optically allowed excited state is denoted by S_1 and is the one-exciton state of the dye. The transition energy between these two states is E_m^e. Let S_n denote the excited state of the dye having the allowed optical transition from the state S_1 whose energy lies closest to $2E_m^e$. Its energy can be written as $2E_m^2 + \Delta_m$, where Δ_m accounts for the energy mismatch. Because the energy of this state is approximately twice that of the state S_1, it can be regarded as the state for which two excitons reside on the dye. The anharmonicity parameter thus provides a simple means to account for the existence of dye energy levels above the first excited state that play a role when more than one exciton is present in the aggregate. $K_{(m,n)}$ is the exciton–exciton interaction energy between an exciton residing on dye m and an exciton residing on dye n. This interaction results from the difference in the charge density of a dye molecule when it is in its excited state compared to when it is in its ground state [34]. This results in a difference in the total Coulomb energy of the aggregate when two excitons reside on neighboring dyes or are farther apart.

These phenomenological parameters are amenable to engineering. The value of E_m^e depends on the dye structure and can be varied by changing substituents on the dye. $J_{(m,n)}$ and $K_{(m,n)}$ depend on the structure of dyes m and n and how the dyes are positioned and oriented with respect to each other. As indicated in the **Appendix**, dye pairs exist for which $J_{(m,n)}$ and $K_{(m,n)}$ can be adjusted independently of each other by reorienting the dyes. In what follows it is assumed that dye aggregate systems can be engineered in which these phenomenological parameters, for nearest neighbor dyes pairs, can take on any desired value within the maximal limits of these quantities for available dyes. Values of E_m^e are in the several electron volt (eV) range. For dye pairs in close proximity, $J_{(m,n)}$ can be in the 100 meV range [10]. On dimensional grounds, one expects that $K_{(m,n)}$ can achieve similar strength. As discussed in the **Appendix**, the strengths of $J_{(m,n)}$ and $K_{(m,n)}$ can be estimated from dipole approximations. In this approximation, $J_{(m,n)}$ is proportional to the product of the transition dipole moments μ_m and μ_n for the two dyes m and n, whereas $K_{(m,n)}$ is proportional to the product of the dipole moments Δd_m and Δd_n. These latter dipoles are referred to as excess dipoles in reference [36] and represent the difference between the excited-state and ground-state charge densities for the two molecules. μ_m and Δd_m can both range as high as 16 debye [36–38]. The values of $J_{(m,n)}$ and $K_{(m,n)}$ can be larger than the characteristic room-temperature thermal energy $k_b T = 26$ meV, where k_B is the Boltzmann constant and T is the absolute temperature of $\sim$300 K. This means that exciton-based quantum gates should function at room temperature, in contrast to superconducting device-based quantum computers that require millikelvin temperatures to operate.

The $B_m^\dagger$ and B_m are not numerical quantities but operators referred to as exciton creation operators and exciton annihilation operators, respectively. These are best viewed as part of a clever and economical bookkeeping formalism that enables the construction of the exciton state space and aids in keeping track of how the state vector changes with time.

At this point it is useful to introduce the notion of an energy eigenstate and an energy eigenvalue. By direct substitution it can be shown that states of the form

$$|\psi\rangle = \mathrm{e}^{-iE_k t/\hbar}|E_k\rangle, \tag{28}$$

where $|E_k\rangle$ is time independent, are solutions to the Schrödinger equation Eq. (1) provided the equation

$$E_k|E_k\rangle = H|E_k\rangle \tag{29}$$

is satisfied. A state satisfying Eq. (29) is said to be an energy eigenstate and E_k is said to be its energy eigenvalue. If the state space is N dimensional N orthogonal energy eigenstates will exist, enumerated by the integer subscripts k.

An aggregate system will have a lowest energy state in which all the dye molecules are in their ground state. This state is denoted by $|0\rangle$ and is taken to have unit norm $\langle 0|0\rangle = 1$. The annihilation operator B_m has the property that

$$B_m|0\rangle = 0. \tag{30}$$

Using this equation one immediately obtains

$$H|0\rangle = 0. \tag{31}$$

It follows that $|0\rangle$ is an energy eigenstate having energy eigenvalue 0. Hence, the Hamiltonian Eq. (27) has been constructed so that the zero of its energy scale matches the ground-state energy of the aggregate.

It is now useful to introduce the notion of a commutator. Given any two operators A and B, their commutator is defined by

$$[A, B] \equiv AB - BA. \tag{32}$$

The exciton creation and annihilation operators satisfy the commutation relations

$$[B_m, B_n] = [B_m^\dagger, B_n^\dagger] = 0 \tag{33}$$

and

$$[B_m, B_n^\dagger] = \delta_{m,n} \tag{34}$$

where $\delta_{m,n}$ is the Kronecker delta function. The Kronecker delta function has the value 0 when $m \neq n$ and the value 1 when $m = n$.

A complete set of orthonormal basis vectors can be constructed by applying products of creation operators to $|0\rangle$. The general state will have the form

$$|n_1, n_2, \ldots, n_N\rangle = \prod_{m=1}^{N} \frac{(B_m^\dagger)^{n_m}}{\sqrt{n_m!}} |0\rangle. \tag{35}$$

The number n_m is the number of excitons residing on dye m.

As the notation for the creation and annihilation operators suggest, $B_m^\dagger$ is regarded as the Hermitian adjoint of B_m. In addition, the Hermitian adjoint of $|0\rangle$ is denoted by $\langle 0|$. Hence, the Hermitian adjoint of the state vector Eq. (35) is given by

$$\langle n_1, n_2, \ldots, n_N| = \langle 0| \prod_{m=1}^{N} \frac{(B_m)^{n_m}}{\sqrt{n_m!}} \tag{36}$$

where use has been made of the commutation relation Eq. (33), allowing reordering of annihilation operators among themselves. Using the commutation relations for the creation and annihilation operators, one can show that these states satisfy the orthonormality condition

$$\langle n_1, n_2, \ldots, n_N | n_1', n_2', \ldots, n_N' \rangle = \prod_{k=1}^{N} \delta_{n_k, n_k'}. \tag{37}$$

The Hamiltonian and the state space have now been described. This system belongs to a class of Hamiltonians referred to as Bose–Hubbard models [20]. It has been shown that universal quantum computation can be performed by a many-particle quantum walk in such systems [20]. The proof consists of showing how a universal set of quantum gates can be implemented in such systems. A similar analysis will be presented here by exhibiting a set of gates that may be easier to implement in dye aggregate systems.

Before doing so, an analysis of a two-dye aggregate is performed to illustrate how computations are carried out with this formalism and to provide some insight into the quantum behavior of excitons.

5 Energy Eigenvalues of a Homodimer Dye Aggregate and Davydov Splitting

Here, as an example of how Frenkel exciton computations are carried out, the energy eigenvalues and eigenvectors of a dye aggregate consisting of two identical dyes (homodimer) are solved for the case when a dye aggregate contains one exciton. It will be shown that as a result of exciton exchange, the absorption spectrum of the dimer exhibits peak splitting, a phenomenon referred to as exciton splitting [39] or Davydov splitting [40].

Consider the case when the dye aggregate consists of two identical dye molecules. The Hamiltonian Eq. (27) then reduces to [41]

$$H = E^e \left(B_1^\dagger B_1 + B_2^\dagger B_2 \right) + J \left(B_1^\dagger B_2 + B_2^\dagger B_1 \right) + \frac{\Delta}{2} \left(B_1^\dagger B_1^\dagger B_1 B_1 + B_2^\dagger B_2^\dagger B_2 B_2 \right) + K B_1^\dagger B_2^\dagger B_2 B_1. \tag{38}$$

The Hamiltonian of Eq. (27) and, consequently, of Eq. (38) is exciton number conserving. That these cannot change the number of excitons follows from the fact that in each term of the Hamiltonian each creation operator is paired with an annihilation operator and from the commutation relations for the exciton creation and annihilation operators. As a consequence, the energy eigenvalues can be found by working with state spaces having a fixed number of excitons. The system ground state $|0\rangle$ is the zero exciton example of this as it is an energy eigenstate.

From Eq. (35), the set of one-exciton states in the site basis is

$$\mathbf{B}_1 = \left\{ B_1^\dagger |0\rangle,\ B_2^\dagger |0\rangle \right\}. \tag{39}$$

These two states are the states in which the exciton occupies molecule 1 or molecule 2, respectively. The set of two-exciton states in the site basis is

$$\mathbf{B}_2 = \left\{ \frac{B_1^\dagger B_1^\dagger}{\sqrt{2}} |0\rangle,\ B_1^\dagger B_2^\dagger |0\rangle,\ \frac{B_2^\dagger B_2^\dagger}{\sqrt{2}} |0\rangle \right\}. \tag{40}$$

The leftmost state of this set is that for which both excitons reside on molecule 1. The middle state is that for which one exciton resides on molecule 1 and the other on molecule 2. The rightmost state is that for which both excitons reside on molecule 2. Note that due to the commutation relation Eq. (33), the state $B_1^\dagger B_2^\dagger |0\rangle$ and the state $B_2^\dagger B_1^\dagger |0\rangle$ are the same state. Thus, only one appears in the set. The formalism via the commutation relations Eqs. (33) and (34), thus, has the indistinguishability of excitons built into it. Indistinguishable particles for which these commutation relations apply satisfy Bose statistics and are referred to as Bosons.

To determine the energy eigenstates and eigenvalues of Hamiltonian Eq. (38) it is useful to evaluate the expression $B_r^\dagger B_s B_t^\dagger |0\rangle$ and $B_s^\dagger B_r^\dagger B_r B_s B_t^\dagger |0\rangle$, where r, s and t are integer site labels. From the commutation relation Eq. (34) one has

$$B_s B_t^\dagger - B_t^\dagger B_s = \delta_{s,t} \tag{41}$$

or

$$B_s B_t^\dagger = \delta_{s,t} + B_t^\dagger B_s. \tag{42}$$

One thus has

$$B_r^\dagger B_s B_t^\dagger |0\rangle = B_r^\dagger \left[\delta_{s,t} + B_t^\dagger B_s \right] |0\rangle = \delta_{s,t} B_r^\dagger |0\rangle \tag{43}$$

and

$$B_s^\dagger B_r^\dagger B_r B_s B_t^\dagger |0\rangle = B_s^\dagger B_r^\dagger B_r \left[\delta_{s,t} + B_t^\dagger B_s\right] |0\rangle = 0 \tag{44}$$

where in each case the last equality follows from Eq. (30). A consequence of the last equation is that terms with the Δ and K coefficients of Eq. (38) are zero in the one-exciton sector of the state space, as one would expect given these terms account for exciton–exciton interactions. Using these last two equations one finds

$$H B_1^\dagger |0\rangle = E^e B_1^\dagger |0\rangle + J B_2^\dagger |0\rangle \tag{45}$$

and

$$H B_2^\dagger |0\rangle = J B_1^\dagger |0\rangle + E^e B_2^\dagger |0\rangle. \tag{46}$$

The general one-exciton state vector has the form

$$|\psi\rangle = \alpha_1 B_1^\dagger |0\rangle + \alpha_2 B_2^\dagger |0\rangle. \tag{47}$$

See Eqs. (4) and (12). Hence, in matrix form one has

$$H|\psi\rangle = \begin{bmatrix} E^e & J \\ J & E^e \end{bmatrix} \begin{bmatrix} \alpha_1 \\ \alpha_2 \end{bmatrix}. \tag{48}$$

Equation (29) becomes

$$E_k \begin{bmatrix} \alpha_{k1} \\ \alpha_{k2} \end{bmatrix} = \begin{bmatrix} E^e & J \\ J & E^e \end{bmatrix} \begin{bmatrix} \alpha_{k1} \\ \alpha_{k2} \end{bmatrix}. \tag{49}$$

The solutions to this eigenvalue–eigenvector equation can be solved by brute force using general linear algebra techniques. The clever approach, however, is to note the Hamiltonian Eq. (38) remains unchanged (is symmetric) under the interchange of subscripts 1 and 2 on the creation and annihilation operators, a consequence of having chosen the two dyes to be identical. In this case it follows from group representation theory of the permutation group that the eigenstates must be symmetric or antisymmetric (changes sign) under the interchange of the site subscripts. Hence, the eigenstates can be immediately written down:

$$|S\rangle = \frac{1}{\sqrt{2}} \left(B_1^\dagger |0\rangle + B_2^\dagger |0\rangle\right) = \frac{1}{\sqrt{2}} \begin{bmatrix} 1 \\ 1 \end{bmatrix} \tag{50}$$

and

$$|A\rangle = \frac{1}{\sqrt{2}} \left(B_1^\dagger |0\rangle - B_2^\dagger |0\rangle\right) = \frac{1}{\sqrt{2}} \begin{bmatrix} 1 \\ -1 \end{bmatrix}, \tag{51}$$

where the state labels S and A indicate whether the state is symmetric or antisymmetric under interchange of the site labels. The corresponding energy eigenvalues are then immediately obtained by substitution of the eigenstates into Eq. (49). One finds

$$E_S = E^e + J \tag{52}$$

and

$$E_A = E^e - J. \tag{53}$$

When the exchange energy J is zero, such as when the dyes are far apart, the energies become degenerate with both eigenstates having the energy E^e. This is the energy of the photon that by absorption in a dye molecule induces a transition from the ground state to its lowest optically allowed excited state. When the exchange energy is nonzero, the energy of the two eigenstates differs by 2J. The transition from the ground state $|0\rangle$ to the excited state $|S\rangle$ is induced by a photon having the energy $E^e + J$. The transition from the ground state to the excited state $|A\rangle$ is induced by a photon having the energy $E^e - J$. The absorption spectrum of the dimer will thus exhibit two peaks in the absorption spectrum, whereas a single dye molecule would exhibit a single absorption peak. This peak splitting is called Davydov splitting and is of size $2J$. Figure 2 provides an experimental example of Davydov splitting observed for two "squaraine-rotaxane" dyes confined to the core of a DNA Holliday junction by covalent linkages [42]. One sees that the absorbance peak of this dimer aggregate is split into two peaks, one on either side of the monomer (single dye) absorbance peak.

Note that for the energy eigenstates Eqs. (50) and (51), the probability amplitude is of equal magnitude for the exciton to reside on dye 1 and dye 2. The exciton acts as if it has a simultaneous existence on both dyes. This is referred to as exciton delocalization. A classical particle would not be able to do this because it can only have one position at a time.

6 Coherent Exciton Hopping

The energy eigenstates at any instant of time make a perfectly good basis set with which to express a quantum state. This basis set is particularly convenient to work with when considering the time evolution of a system. Any state $|\psi(0)\rangle$ can be expressed in the form

$$|\psi(0)\rangle = \sum_{k=1}^{N} \alpha_k |E_k\rangle, \tag{54}$$

where $|E_k\rangle$ are the energy eigenstates obtained by solving Eq. (29). Using this as the initial condition for the state $|\psi\rangle$ appearing in the Schrödinger equation Eq. (7) the solution to the Schrödinger equation is given by

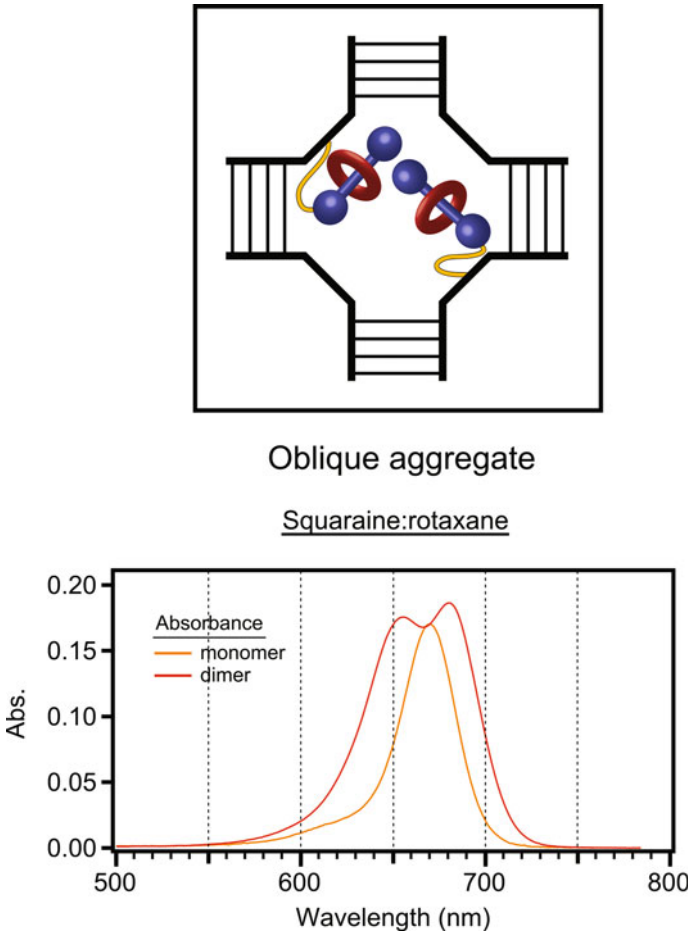

Fig. 2 A dimer dye aggregate whose absorbance spectrum exhibits Davydov splitting. The aggregate consists of two "squaraine-rotaxane" dyes (SeTau-670 from SETA BioMedicals) confined to the core of a DNA Holliday junction by covalent linkages, as shown schematically in the top panel. In the bottom panel, the absorbance spectrum of the monomer dye shows a single peak, whereas that of the dimer aggregate shows two peaks, one on either side of the monomer absorbance peak. Based on absorbance and circular dichroism data it was determined that the dyes make an angle of about 85° with respect to each other, a configuration referred to as oblique. Figure panels modified are from Barclay et al. [42]

$$|\psi(t)\rangle = \sum_{k=1}^{N} \alpha_k \mathrm{e}^{-iE_k t/\hbar} |E_k\rangle. \tag{55}$$

As an example of the time dependence that a homodimer aggregate may exhibit, consider the case when at $t = 0$ the state vector is given by

$$|\psi(0)\rangle = \frac{1}{\sqrt{2}}(|S\rangle + |A\rangle). \tag{56}$$

Substituting Eqs. (50) and (51) into this equation yields

$$|\psi(0)\rangle = B_1^\dagger|0\rangle. \tag{57}$$

The initial state Eq. (56) is the state in which the exciton resides only on dye 1. Such a state can be prepared for a dye aggregate in which the two dye molecules have a different orientation. In this case, the polarization of a femtosecond laser light pulse can be oriented so that it is orthogonal to the dipole component of the transition charge density of molecule 2 but not that of dye 1. In this manner, the laser light pulse can only induce an optical transition from the ground state to the lowest optically allowed excited state in dye 1 [18].

As indicated by Eq. (55), the time evolution of this state is given by

$$|\psi(t)\rangle = \frac{1}{\sqrt{2}}\left(\mathrm{e}^{-iE_St/\hbar}|S\rangle + \mathrm{e}^{-iE_At/\hbar}|A\rangle\right). \tag{58}$$

Substitution of Eqs. (50) through (53) into this equation yields

$$|\psi(t)\rangle = \mathrm{e}^{-iE^et/\hbar}\left[\cos\left(\frac{Jt}{\hbar}\right)B_1^\dagger|0\rangle - 2i\sin\left(\frac{Jt}{\hbar}\right)B_2^\dagger|0\rangle\right]. \tag{59}$$

From this, it is evident that the probability of finding the exciton on dye 1 as a function of time is

$$P_1(t) = \cos^2\left(\frac{Jt}{\hbar}\right), \tag{60}$$

whereas the probability of finding the exciton on dye 2 is given by

$$P_2(t) = \sin^2\left(\frac{Jt}{\hbar}\right). \tag{61}$$

Hence, at the instances of time $t = n\pi\hbar/J$, where n is an integer, the exciton resides entirely on dye 1; at the instances of time $(n + 1/2)\pi\hbar/J$, the exciton resides entirely on dye 2. The exciton thus hops back and forth between the two dyes with a frequency of $\pi\hbar/J$. Optical experiments using femtosecond light pulses are able to reveal such coherent oscillations. This phenomenon is referred to as exciton coherence.

Having discussed exciton delocalization and exciton coherence, we now move on to exciton devices.

7 Exciton Transmission Lines

For a many-particle quantum walk-based quantum computer, a means is required to transport particles from the output of one gate to the input of the next. Here it is shown that a dye aggregate consisting of a linear array of molecules can function as an exciton transmission line and thus can serve as a wire connecting gates [43].

For simplicity, consider an infinite array of identical dye molecules equally spaced and the case when only one exciton is present. One can then drop the exciton–exciton interaction terms of the Hamiltonian Eq. (27) and the Hamiltonian becomes

$$H = E^{\mathrm{e}} \sum_{r=-\infty}^{\infty} B_r^\dagger B_r + J \sum_{m=-\infty}^{\infty} (B_{r+1}^\dagger B_r + B_r^\dagger B_{r+1}) \tag{62}$$

where, for simplicity, all but nearest neighbor interactions have also been neglected, an approximation that is generally satisfactory because $J_{m,n}$ falls off as the reciprocal of the cube of the distance between dyes m and n.

The system is invariant under translation by the lattice spacing. Group representation theory then indicates that the one-exciton energy eigenstates must have the Bloch form

$$|k\rangle = \frac{1}{\sqrt{2\pi}} \sum_{r=-\infty}^{\infty} \mathrm{e}^{ikr} B_r^\dagger |0\rangle, \tag{63}$$

where k is a real number restricted to the range $-\pi < k \leq \pi$ due to the periodic nature of the functions e^{ikr}. Applying this state to the Hamiltonian Eq. (62) yields

$$H|k\rangle = \left[E^e + 2J\cos(k)\right]|k\rangle, \tag{64}$$

demonstrating directly that $|k\rangle$ is a eigenstate of the Hamiltonian Eq. (62) having the energy eigenvalue

$$E_k = E^e + 2J\cos(k). \tag{65}$$

The general one-exciton state for an exciton residing on the dye array has the form

$$|\psi(t)\rangle = \frac{1}{\sqrt{2\pi}} \int_{-\pi}^{\pi} \mathrm{d}k\ f(k)\mathrm{e}^{-iE_k t/\hbar}|k\rangle, \tag{66}$$

where $f(k)$ is a complex function of k. This is a generalization of Eq. (55) for the case when the state label is a continuous variable rather than a member of a discrete set. Introducing the frequencies

$$\omega_k = \frac{E_k}{\hbar};\ \omega_e = \frac{E^e}{\hbar};\ \text{and}\ \omega_J = \frac{J}{\hbar}, \tag{67}$$

the dispersion relation Eq. (65) can be written as

$$\omega_k = \omega_e + 2\omega_J \cos(k) \tag{68}$$

and Eq. (66), with the aid of Eq. (63), can be put into the form

$$|\psi(t)\rangle = \frac{1}{2\pi} \sum_{r=-\infty}^{\infty} \int_{-\pi}^{\pi} f(k) \mathrm{e}^{-i(\omega_k t - kr)} \mathrm{d}k B_r^\dagger |0\rangle. \tag{69}$$

In this form, it is evident that the general one-exciton state consists of a wave packet of waves with an oscillatory function of time and position along the dye array given by $\mathrm{e}^{-i(\omega_k t - kr)}$. Thus, the exciton propagates along the transmission line in a wave-like manner.

When $f(k)$ is strongly peaked with a narrow width about a particular k, the concept of wave packet velocity (known as group velocity) becomes meaningful and is given by

$$v_g \equiv a \frac{\partial \omega_k}{\partial k}, \tag{70}$$

where a is the lattice spacing (the nearest neighbor distance between the dyes). From Eq. (68) one obtains

$$v_g = -2\omega_J a \sin(k). \tag{71}$$

The magnitude of the group velocity is greatest when

$$k = \pm \frac{\pi}{2} \tag{72}$$

and has the value $2\omega_J a$. This is the speed limit for signals propagating along the transmission line.

Because an exciton wave with definite k has the oscillatory form $\mathrm{e}^{-i(\omega_k t - kr)}$, one sees that at the group velocity maximum the wavelength of the exciton is four lattice units long. A quarter wavelength or $\pi/2$ phase shift is present between two neighboring dyes at any instant of time. This observation will play a significant role in the discussion of exciton-based basis change gates.

8 Representation of an Exciton Qubit

In the design of quantum computers, a decision needs to be made on how information is to be encoded in the physical hardware. An obvious choice for excitons undergoing a many-particle quantum walk over a dye aggregate would be to let the absence of an exciton denote a logical 0 and the presence of an exciton denote a logical 1. Because

the exciton can exist in a superposition of being present or absent, this is a qubit. This is the representation that Childs et al. [20] chose in their proof that universal quantum computation can be implemented in Bose–Hubbard systems.

Here an alternative encoding will be employed where a qubit is carried by two transmission lines, say lines 1 and 2. If the exciton is on line 1 that is to be regarded as a logical 0. If it is on line 2 that is to be regarded as a logical 1. This is referred to as the "dual-rail" mode of operation. The exciton can be in a superposition state for which there is a probability amplitude α_1 of its being on line 1 and a probability amplitude α_2 of its being on line 2, so this coding indeed implements a qubit. This dual-rail representation of a qubit enables the simplification of gate design but at the cost of having twice as many wires (exciton transmission lines) connecting the gates.

9 Basis Change Gates

We now consider aggregates that function as quantum gates. These aggregates are connected to exciton transmission lines that supply the input signals and deliver the output. A general mathematical framework is developed before considering specific gates.

Equation (63) suggests that one introduces the annihilation operator

$$B(k) = \frac{1}{\sqrt{2\pi}} \sum_{r=-\infty}^{\infty} \mathrm{e}^{ikr} B_r. \tag{73}$$

Its Hermitian conjugate is a creation operator which, when operating on $|0\rangle$, produces a one-exciton state with wave vector k and frequency ω_k. It is an energy eigenstate with the energy eigenvalue $E_k = \hbar\omega_k$ given by Eq. (65). A consequence of the infinite sum in Eq. (73) and the continuous nature of the index k is that these creation and annihilation operators satisfy the commutation relations

$$\left[B(k), B(k')\right] = 0 \tag{74}$$

and

$$[B(k), B^\dagger(k')] = \delta(k - k'), \tag{75}$$

where $\delta(k - k')$ is a functional referred to as the Dirac delta function.

The exciton of state $B^\dagger(-k)|0\rangle$ propagates in the opposite direction from the exciton of state $B^\dagger(k)|0\rangle$.

We now consider the case of a one-qubit gate. In the dual-rail representation, this gate will have two transmission lines carrying the input qubit and two transmission lines carrying the output qubit. The situation is depicted in Fig. 3. Because signals can propagate both ways on each transmission line, we must consider eight annihilation operators. We employ the labelings $B^\alpha_\beta(k)$ where the superscript $\alpha \in \{\text{in}, \text{ out}\}$

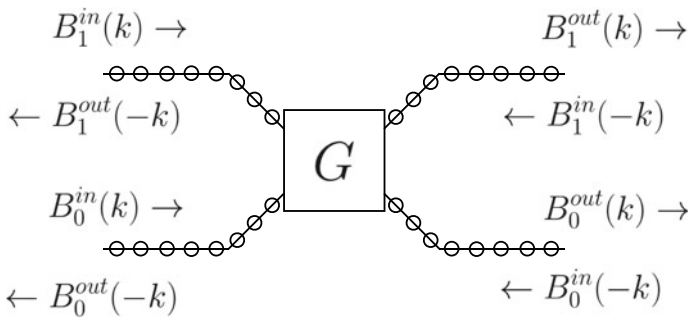

Fig. 3 A general one qubit gate G connected to four exciton transmission lines. The transmission lines consist of arrays of dyes that are here represented by circles placed along a line

indicates whether the exciton is propagating "in" toward the gate G or "out" away from the gate. The subscript $\beta \in \{0, 1\}$ indicates whether the exciton resides on the logical 0 or the logical 1 transmission line of the qubit, and the argument k indicates the value of the wave vector.

Consider the case when all the transmission lines have the same E^e and J. The exciton associated with the exciton creation operator $B_1^{\text{in}}(k)$, after arriving at the gate G, will exit one of the four outputs $B_0^{\text{out}}(k)$, $B_1^{\text{out}}(k)$, $B_0^{\text{out}}(-k)$ and $B_1^{\text{out}}(-k)$. Because energy is conserved and the transmission lines are identical, if the incoming exciton has wave vector k, the outgoing exciton can only have the wave vector k or $-k$. Hence, one need only consider the annihilation operators shown in Fig. 3. One has a similar situation with excitons entering the other input ports. The relation between the input and output annihilation operators is given by

$$\begin{bmatrix} B_1^{\text{out}}(k) \\ B_0^{\text{out}}(k) \\ B_1^{\text{out}}(-k) \\ B_0^{\text{out}}(-k) \end{bmatrix} = \begin{bmatrix} S_{11} & S_{12} & S_{13} & S_{14} \\ S_{21} & S_{22} & S_{23} & S_{24} \\ S_{31} & S_{32} & S_{33} & S_{34} \\ S_{41} & S_{42} & S_{43} & S_{44} \end{bmatrix} \begin{bmatrix} B_1^{\text{in}}(k) \\ B_0^{\text{in}}(k) \\ B_1^{\text{in}}(-k) \\ B_0^{\text{in}}(-k) \end{bmatrix}. \tag{76}$$

The matrix elements $S_{m,n}$ are, in general, complex numbers. The square matrix containing the $S_{m,n}$ is referred to as a scattering matrix. Let this matrix be denoted by **S**. Because the incoming signals are independent, the "in" creation and annihilation operators must satisfy commutation relations similar to those of Eqs. (71) and (72)

$$[B_\beta^{\text{in}}(k), B_{\beta'}^{\text{in}}(k')] = 0 \tag{77}$$

and

$$[B_\beta^{\text{in}}(k), B_{\beta'}^{in\dagger}(k')] = \delta_{\beta,\beta'}\delta(k - k'). \tag{78}$$

Similarly the outgoing singles are linearly independent of each other and consequently the "out" creation and annihilation operators also satisfy commutation rela-

tions of the form Eqs. (77) and (78). For all these commutation relations to be satisfied, the matrix **S** must be unitary. That **S** be unitary is also required by the conservation of energy and is a manifestation of the unitary evolution imposed by the Schrödinger equation.

When the device simply consists of two parallel transmission lines that are sufficiently far apart that exciton hopping from one transmission line to the other does not occur there is no scattering and the **S** matrix is diagonal

$$\mathbf{S} = \begin{bmatrix} 1\,0\,0\,0 \\ 0\,1\,0\,0 \\ 0\,0\,1\,0 \\ 0\,0\,0\,1 \end{bmatrix}. \tag{79}$$

When two exciton transmission lines are brought sufficiently close so that the oscillatory Coulomb interaction can occur between between dye pairs, with one dye located on each transmission line, an exciton can hop from one transmission line to the other. Thereby nondiagonal entries of the **S** array become nonzero.

To make a specific quantum gate, such as a Hadamard gate, the challenge is to engineer a dye aggregate that produces the desired matrix elements $S_{m,n}$. For this, the electrical engineering literature on distributed element circuits serves as a useful guide. These radio frequency and microwave circuits are based on wave interference. In these circuits, transmission line segments a quarter of a wavelength long play a prominent role. One such device is shown in Fig. 4a. It is an example of a branch line coupler [44]. Signals entering port 1 of this coupler exit ports 2 and 3, and no signal exits port 4. For the case shown, the transmission line segments that are narrow have a transmission line impedance of Z_0, whereas the two transmission line segments that are wide have a transmission line impedance of $Z_0/\sqrt{2}$. With these impedance values, the signal entering port 1 is split evenly between ports 2 and 3, that is, the device functions as a 50/50 beam splitter. Because distributed element circuits rely on wave interference they generally function well over a limited range of wavelengths (or frequencies) centered about a midband wavelength (or frequency) determined by the length of the transmission line segments.

The device shown in Fig. 4b is a direct translation of the device of Fig. 4a into an exciton device. Because there is a quarter wavelength shift in the phase between neighboring dyes at the band center $k = \pi/2$, the distance between the dyes in effect serves as a quarter wavelength section of transmission line. The energy parameter J plays the role of the reciprocal of impedance. Because the value of J depends on the spacing between dyes, the dye spacing can be adjusted to yield the desired value. In this case, the coupling between all nearest neighbor dyes is J except for the two having the value $\sqrt{2}J$, as indicated in the figure by arrows.

At band center, the scattering matrix Eq. (73) for this device is

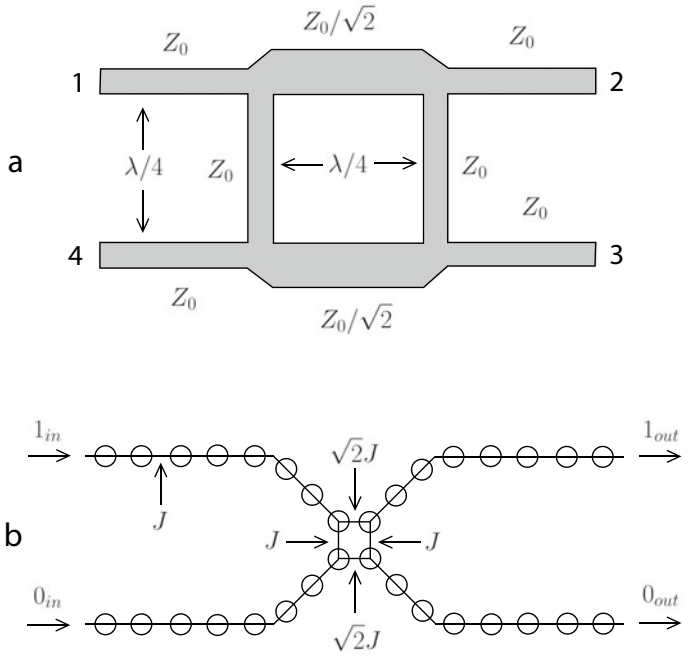

Fig. 4 A branch line coupler as implemented in radio and microwave frequency electronics (**a**) and as an exciton device implemented using dye molecules (**b**). For the values of the impedance or exciton exchange energies shown, these devices act as 50/50 power dividers. The exciton device (**b**) functions as a basis change gate

$$\mathbf{S} = \frac{1}{\sqrt{2}} \begin{bmatrix} i & 1 & 0 & 0 \\ 1 & i & 0 & 0 \\ 0 & 0 & i & 1 \\ 0 & 0 & 1 & i \end{bmatrix}. \tag{80}$$

From the zeros in this matrix, it is evident that signals entering ports B_1^{in} and B_0^{in} are only delivered to ports B_1^{out} and B_0^{out}. Hence, the device can be regarded as a one-qubit gate in which the input enters the left side of the device and the output exits the right side as shown in Fig. 4b, where the logical 1 and logical 0 lines have been indicated. The transformation performed on the annihilation operators is

$$\begin{bmatrix} B_1^{\text{out}} \\ B_0^{\text{out}} \end{bmatrix} = \frac{1}{\sqrt{2}} \begin{bmatrix} i & 1 \\ 1 & i \end{bmatrix} \begin{bmatrix} B_1^{\text{in}} \\ B_0^{\text{in}} \end{bmatrix}. \tag{81}$$

This transformation can be inverted to express the annihilation operators of the incoming signals in terms of the annihilation operators of the outgoing signals.

$$\begin{bmatrix} B_1^{\text{in}} \\ B_0^{\text{in}} \end{bmatrix} = \frac{1}{\sqrt{2}} \begin{bmatrix} -i & 1 \\ 1 & -i \end{bmatrix} \begin{bmatrix} B_1^{\text{out}} \\ B_0^{\text{out}} \end{bmatrix}. \tag{82}$$

Consider the case when the state of the system $|\psi_S\rangle$ is that for which the incoming signal is a logical 1:

$$|\psi_S\rangle = B_1^{\text{in}\dagger}|0\rangle. \tag{83}$$

From Eq. (82), one has

$$B_1^{\text{in}} = \frac{1}{\sqrt{2}} \left(B_1^{\text{out}} - i B_0^{\text{out}} \right). \tag{84}$$

Substituting this into Eq. (83) and remembering that taking the Hermitian adjoint involves complex conjugation one obtains

$$|\psi_S\rangle = \frac{1}{\sqrt{2}} \left(B_1^{\text{out}\dagger}|0\rangle + i B_0^{\text{out}\dagger}|0\rangle \right). \tag{85}$$

Hence, this system state is one for which the exciton exits the gate as a superposition state in which the probability amplitude that the exciton is on the logical 1 line is $1/\sqrt{2}$ and the probability amplitude that the exciton is on the logical 0 line is $i/\sqrt{2}$.

The gate of Fig. 4b is capable of exhibiting the ideal performance of Eq. (81) at the transmission line band center $k = \pm\pi/2$; however, its performance degrades away from band center. But the degradation is graceful in that there is a finite bandwidth over which the device functions satisfactorily for any specified tolerance level. A full analysis of this gate is presented in [43]. Greater bandwidth than that exhibited by the gates of Fig. 4 can be achieved with more complex gate designs, the theory of which is well developed for distributed element circuits.

10 Phase Gates

Phase shifts can be implemented as propagation delays. Figure 5 illustrates two transmission lines along which a qubit in the dual-rail representation propagates. For the phase gate shown in Fig. 5, one line has been made one dye longer than the other. For signals propagating at the midband of the transmission line, this extra length induces a quarter wavelength propagation delay (a $\pi/2$ phase shift) with respect to the shorter transmission line. The transformation performed by this gate is given by

$$\begin{bmatrix} B_1^{\text{out}} \\ B_0^{\text{out}} \end{bmatrix} = \begin{bmatrix} \mathrm{e}^{\mathrm{i}\pi/2} & 0 \\ 0 & 1 \end{bmatrix} \begin{bmatrix} B_1^{\text{in}} \\ B_0^{\text{in}} \end{bmatrix}. \tag{86}$$

Propagation delays can be induced by other means. From Eq. (63), it is evident that the phase factor between neighboring dyes is e^{ik}, that is, the phase shift is k. Taking the energy E_k of the exciton (or the carrier frequency ω_k of the signal) to

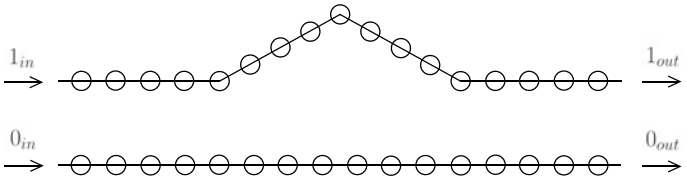

Fig. 5 A phase gate consisting of two transmission lines. The phase shift results from propagation a delay of the signal traveling over the longer transmission line. For the case shown, where one transmission line is one dye longer than the other, the phase shift is $\pi/2$ at the transmission line midband

be the controlling variable, the value of k is obtained by solving Eq. (65). One sees that it depends on E^e and J. Hence, phase shifts can be induced by having E^e or J differ in sections of one transmission line by employing different dyes (changes E^e and J) or by changing the spacing between neighboring dyes (changes J). We thus posit that any phase gate of the form of Eq. (18) can be engineered.

It is now shown how the basis change gate exhibited in Eq. (81),

$$U_B = \frac{1}{\sqrt{2}} \begin{bmatrix} i & 1 \\ 1 & i \end{bmatrix}, \tag{87}$$

can be converted into a Hadamard gate by sandwiching it between two phase gates of the form

$$U_P = \begin{bmatrix} \mathrm{e}^{-i\pi/4} & 0 \\ 0 & \mathrm{e}^{i\pi/4} \end{bmatrix}. \tag{88}$$

Carrying out the matrix multiplication

$$U_H = U_P U_B U_P \tag{89}$$

one finds that U_H is the Hadamard gate Eq. (17).

An alternative means of implementing a Hadamard gate would be to translate a hybrid ring coupler, also called a rat-race coupler [44], (a distributed element circuit device) into an exciton device as was done for the branch line coupler of Fig. 4.

11 An Exciton Interferometer

As an illustration of how single qubit gates can be composed to produce new single qubit gates, exciton interferometers will now be discussed. This will also lay the foundation for a discussion of the CNOT gate. An exciton interferometer can be constructed as a phase gate sandwiched between two basis change gates. As an

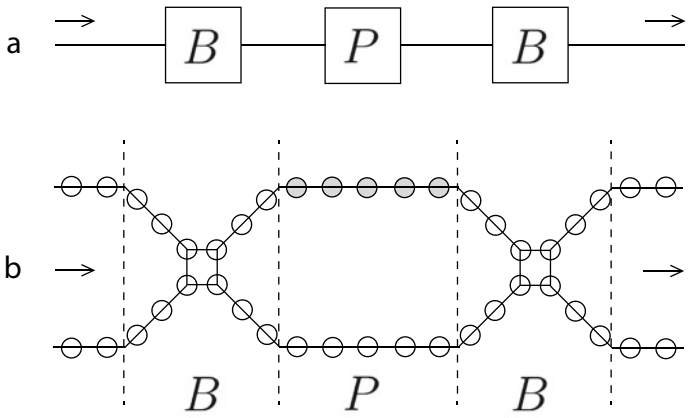

Fig. 6 An exciton interferometer. **a** A schematic representation of the device as a cascade of a branch line coupler gate, a phase gate and a second branch line coupler. **b** The physical layout of the dyes forming an interferometer. The upper transmission line of the phase gate has been shaded to indicate that its propagation delay (phase shift) may be different from that of the lower transmission line

example, consider the phase gate of Eq. (18) sandwiched between two basis change gates given by Eq. (87). The configuration is illustrated schematically in Fig. 6a as a cascade of gates, and the physical layout of the dyes is shown in Fig. 6b.

The overall transformation is given by

$$U_I = U_B U_P U_B \tag{90}$$

Carrying out the matrix multiplication yields

$$U_I = i e^{i(\phi_1+\phi_2)/2} \begin{bmatrix} -\sin[(\phi_1-\phi_2)/2] & \cos[(\phi_1-\phi_2)/2] \\ \cos[(\phi_1-\phi_2)/2] & \sin[(\phi_1-\phi_2)/2] \end{bmatrix}. \tag{91}$$

From this, it is evident that how an exciton entering one port of the interferometer is distributed among the output ports depends sinusoidally on the phase difference $\phi_1 - \phi_2$ of the phases of the phase gate. This composition of gates thus functions as an interferometer that is sensitive to the phase difference between the two arms (transmission lines) internal to the interferometer.

To simplify the discussion, consider the case when ϕ_2 has the fixed value π. Then Eq. (91) reduces to

$$U_I(\phi) = -e^{i\phi/2} \begin{bmatrix} \cos(\phi/2) & \sin(\phi/2) \\ \sin(\phi/2) & -\cos(\phi/2) \end{bmatrix}, \tag{92}$$

where we have set $\phi_1 = \phi$.

When $\phi = 0$, this matrix reduces to

$$U(0) = \begin{bmatrix} -1 & 0 \\ 0 & 1 \end{bmatrix}. \tag{93}$$

In this case, an exciton entering on the logical 1 line exits on the logical 1 line and an exciton entering on the logical 0 line exits on the logical 0 line. Hence, for Boolean inputs, the Boolean value remains unchanged as the qubit passes through the interferometer with the setting $\phi = 0$.

When $\phi = \pi$, Eq. (92) reduces to

$$U(\pi) = -i \begin{bmatrix} 0 & 1 \\ 1 & 0 \end{bmatrix}. \tag{94}$$

Now a qubit entering as a logical 1 exits as a logical 0 and a qubit entering as a logical 0 exits as a logical 1. Thus, with the phase ϕ set at π the interferometer acts as a NOT gate. Now, if one had a means to switch ϕ between 0 and π, one would have a controlled NOT gate. How such a switching element can be constructed is discussed next.

12 A Controlled Phase Shift

To convert the interferometer of Fig. 6 into a controlled gate, a controlled phase shifting element is needed in which one exciton controls the phase shift of another. This requires an exciton–exciton interaction. Here the changes in the static Coulomb interaction between dyes resulting from changes in the charge distribution, when a dye transitions from the ground state to the lowest optically allowed excited state, are utilized, that is, the $K_{m,n}$ interactions of Eq. (27) are employed.

A means is required to enable two excitons to interact in a controlled manner. A way to accomplish this is shown in Fig. 7. Shown are two parallel transmission lines that differ such that the group velocity of the upper transmission line is less than that of the lower transmission line. The dyes of the two transmission lines are oriented such that the exchange energy between dyes on separate transmission lines is zero. This prevents the transitioning of an exciton from one transmission line to the other. As discussed in the **Appendix**, since the exciton–exciton interaction energy arises from a different mechanism than of the exchange energy, the inter-transmission line exciton–exciton interaction energy need not be zero even though the exciton exchange energy is. By running the two transmission lines close to each other the inter-transmission line strength K of the exciton–exciton interaction can be made large.

For operation, exciton wave packets are introduced on both transmission lines; however, the packet on the upper transmission line is introduced first to give it a head start as shown in Fig. 7a. The exciton wave packet on the lower transmission line

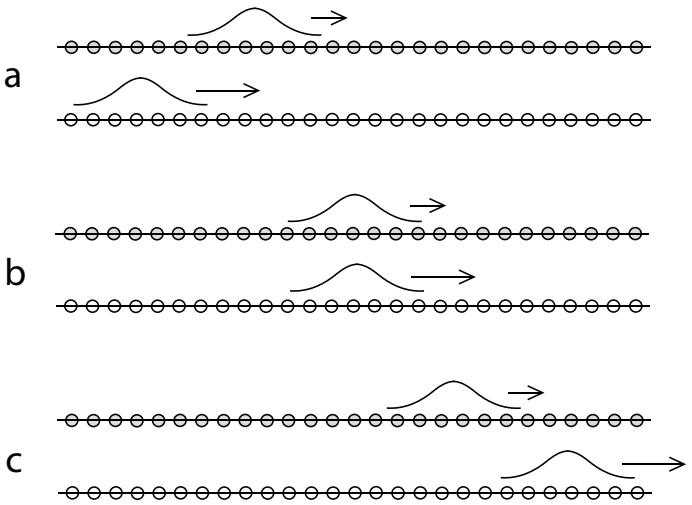

Fig. 7 A controlled phase shifting element. The device consists of two transmission lines which have no inter-transmission line J coupling, but inter-transmission line K coupling, enabling an exciton on one transmission line to change the phase of an exciton on the other transmission line. The dyes of the upper transmission line are shaded to indicate that the signal propagation speed is slower on that transmission line. That enables an exciton wave packet of the lower transmission line to overtake an exciton wave packet of the upper transmission line, as shown at successive time snapshots (**a**), (**b**) and (**c**). Thereby, the two excitons are ensured to interact regardless of where each resides in its wave packet

catches up with the wave packet of the upper transmission line as shown in Fig. 7b and then surpasses it as shown in Fig. 7c. Where the excitons are located in each wave packet is unknown, but, because one wave packet completely overtakes the other, the two excitons are guaranteed to interact. The interaction energy is short range but has the value K when the two excitons are directly across from each other. The phase winding induced by the interaction can be estimated using $\mathrm{e}^{-iKt_I/\hbar}$, where t_I is the time interval over which the excitons interact. Let J_1 and J_2 denote the strength of the hopping interaction for the upper and lower transmission line, respectively, then from the expression for the group velocity at midband Eq. (71) and from Eq. (67), the magnitude of the group velocity difference is

$$\Delta v_g = \frac{2|J_2 - J_1|a}{\hbar}. \tag{95}$$

Because the excitons strongly interact only when they are within a lattice unit a of each other, an estimate of the interaction time is

$$t_I = \frac{a}{|\Delta v_g|} = \frac{\hbar}{2|J_2 - J_1|}. \tag{96}$$

Hence, the phase winding is $e^{-iK/2|J_2-J_1|}$, that is, the phase accumulated during the interaction is

$$\phi_I = -\frac{K}{2|J_2 - J_1|}. \tag{97}$$

The value of ϕ_I can be engineered through choice of K, J_1 or J_2. Let $|\psi_{\text{in}}\rangle$ denote the state of the system before the interaction and $|\psi_{\text{out}}\rangle$ the state of the system after the interaction. The relation between these two states is

$$|\psi_{\text{out}}\rangle = e^{i\phi_I}|\psi_{\text{in}}\rangle. \tag{98}$$

Because the incoming and outgoing states are both two-exciton states and the excitons cannot transition from one transmission line to the other, the exciton–exciton interaction can be expressed in terms of the incoming and outgoing annihilation operators by

$$B_1^{\text{out}} B_2^{\text{out}} = e^{i\phi_I} B_1^{\text{in}} B_2^{\text{in}}. \tag{99}$$

13 A CNOT Gate

Here we consider the CNOT gate shown in Fig. 8. This device is implemented by adding to the interferometer circuit of Fig. 6 two more transmission lines that carry the control qubit. The lower of these two transmission lines comes in close proximity to the transmission line of the upper arm of the interferometer to form the controlled phase shifter discussed in Sect. 12. Here A_m, B_m, C_m and D_m denote the annihilation operators for the right propagating exciton modes at various points in the device. They also serve as position markers within the device. The input exciton modes are denoted by A_m^{in} and the output exciton modes are denoted by D_m^{out}. The controlled phase shifter consists of the parallel transmission line segments B_2–C_2 and B_3–C_3.

The core of the CNOT gate is analyzed first. Because a dual-rail representation is employed, when the control qubit and target qubit enter the device, two excitons are present in device, one residing in the control transmission lines and the other residing in the interferometer. Hence, to analyze the performance of the core of this device, one can restrict the analysis to the state space spanned by the basis set:

$$\mathbf{B}_{CT} = \left\{ A_1^\dagger A_3^\dagger|0\rangle,\ A_1^\dagger A_4^\dagger|0\rangle,\ A_2^\dagger A_3^\dagger|0\rangle,\ A_2^\dagger A_4^\dagger|0\rangle \right\}. \tag{100}$$

Expressed in terms of the $B_m^\dagger$ creation operators, the $A_m^\dagger$ creation operators are given by

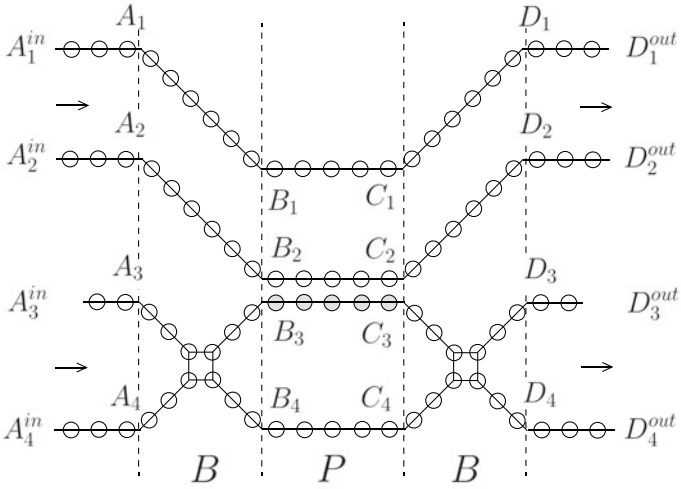

Fig. 8 A controlled NOT gate (CNOT) consisting of an interferometer with one arm coupled to one transmission line of the control qubit transmission line pair to form a controlled phase shift element. The interferometer consists of a branch line coupler B, followed by the phase shifting elements P, followed in turn by a second branch line coupler. Note that the input and output transmission line 3 has been shortened by one dye relative to the other input and output transmission lines. This implements propagation delays that put the scattering matrix of the device in standard form for that of a CNOT gate

$$A_1^\dagger = B_1^\dagger \tag{101}$$
$$A_2^\dagger = B_2^\dagger \tag{102}$$
$$A_3^\dagger = \frac{1}{\sqrt{2}}\left(-i\,B_3^\dagger + B_4^\dagger\right) \tag{103}$$
$$A_4^\dagger = \frac{1}{\sqrt{2}}\left(B_3^\dagger - i\,B_4^\dagger\right). \tag{104}$$

The first two equations express propagation along the control qubit transmission lines. The second two equations express the basis change transformation performed by the first branch line coupler, see Eq. (82). With relationships Eq. (101) through (104), one obtains

$$\begin{aligned}
A_1^\dagger A_3^\dagger &= \frac{1}{\sqrt{2}}\left(-i\,B_1^\dagger B_3^\dagger + B_1^\dagger B_4^\dagger\right)\\
A_1^\dagger A_4^\dagger &= \frac{1}{\sqrt{2}}\left(B_1^\dagger B_3^\dagger - i\,B_1^\dagger B_4^\dagger\right)\\
A_2^\dagger A_3^\dagger &= \frac{1}{\sqrt{2}}\left(-i\,B_2^\dagger B_3^\dagger + B_2^\dagger B_4^\dagger\right)\\
A_2^\dagger A_4^\dagger &= \frac{1}{\sqrt{2}}\left(B_2^\dagger B_3^\dagger - i\,B_2^\dagger B_4^\dagger\right).
\end{aligned} \tag{105}$$

The relationships between $B_m^\dagger$ and $C_m^\dagger$ are now established. Because excitons on transmission lines 1 and 4 do not interact with excitons on the other transmission lines in the region P, one has

$$B_1^\dagger = C_1^\dagger \tag{106}$$

and

$$B_4^\dagger = \mathrm{e}^{i\phi_F} C_4^\dagger \tag{107}$$

where, in writing the last equation, allowance has been made for a fixed propagation delay characterized by the fixed phase ϕ_F that can be engineered to have a desired value. When no exciton exists on transmission line 3, the exciton on transmission line 2 does not interact with excitons on the other transmission lines. In this case

$$B_2^\dagger = C_2^\dagger. \tag{108}$$

One thus has the relations

$$B_1^\dagger B_3^\dagger = C_1^\dagger C_3^\dagger \tag{109}$$

$$B_1^\dagger B_4^\dagger = \mathrm{e}^{i\phi_F} C_1^\dagger C_4^\dagger \tag{110}$$

$$B_2^\dagger B_4^\dagger = \mathrm{e}^{i\phi_F} C_2^\dagger C_4^\dagger. \tag{111}$$

When an exciton exists on each of transmission lines 2 and 3, the two excitons interact, and from Eq. (99) one has

$$B_2^\dagger B_3^\dagger = \mathrm{e}^{i\phi_I} C_2^\dagger C_3^\dagger. \tag{112}$$

The equations of (105) now yield

$$\begin{aligned}
A_1^\dagger A_3^\dagger &= \frac{1}{\sqrt{2}}\left(-iC_1^\dagger C_3^\dagger + \mathrm{e}^{i\phi_F} C_1^\dagger C_4^\dagger\right) \\
A_1^\dagger A_4^\dagger &= \frac{1}{\sqrt{2}}\left(C_1^\dagger C_3^\dagger - i\mathrm{e}^{i\phi_F} C_1^\dagger C_4^\dagger\right) \\
A_2^\dagger A_3^\dagger &= \frac{1}{\sqrt{2}}\left(-ie^{i\phi_I} C_2^\dagger C_3^\dagger + \mathrm{e}^{i\phi_F} C_2^\dagger C_4^\dagger\right) \\
A_2^\dagger A_4^\dagger &= \frac{1}{\sqrt{2}}\left(e^{i\phi_I} C_2^\dagger C_3^\dagger - i\mathrm{e}^{i\phi_F} C_2^\dagger C_4^\dagger\right).
\end{aligned} \tag{113}$$

The mode transformations between $C_m^\dagger$ and $D_m^\dagger$ are similar to those of Eqs. (101) through (104) and will not be presented here. One finds

$$
\begin{aligned}
A_1^\dagger A_3^\dagger &= \frac{1}{2}\left[\left(e^{i\phi_F}-1\right)D_1^\dagger D_3^\dagger - i\left(e^{i\phi_F}+1\right)D_1^\dagger D_4^\dagger\right]\\
A_1^\dagger A_4^\dagger &= \frac{1}{2}\left[-i\left(e^{i\phi_F}+1\right)D_1^\dagger D_3^\dagger - \left(e^{i\phi_F}-1\right)D_1^\dagger D_4^\dagger\right]\\
A_2^\dagger A_3^\dagger &= \frac{1}{2}\left[\left(e^{i\phi_F}-e^{i\phi_I}\right)D_2^\dagger D_3^\dagger - i\left(e^{i\phi_F}+e^{i\phi_I}\right)D_2^\dagger D_4^\dagger\right]\\
A_2^\dagger A_4^\dagger &= \frac{1}{2}\left[-i\left(e^{i\phi_F}+e^{i\phi_I}\right)D_2^\dagger D_3^\dagger - \left(e^{i\phi_F}-e^{i\phi_I}\right)D_2^\dagger D_4^\dagger\right].
\end{aligned}
\tag{114}
$$

Now the fixed phase on transmission line 4 is chosen to be $\phi_F = \pi$ and the interaction-induced phase shift, Eq. (97), is chosen to be $\phi_I = \pi$. The transformation (114) then becomes

$$
\begin{aligned}
A_1^\dagger A_3^\dagger|0\rangle &= -D_1^\dagger D_3^\dagger|0\rangle\\
A_1^\dagger A_4^\dagger|0\rangle &= D_1^\dagger D_4^\dagger|0\rangle\\
A_2^\dagger A_3^\dagger|0\rangle &= i D_2^\dagger D_4^\dagger|0\rangle\\
A_2^\dagger A_4^\dagger|0\rangle &= i D_2^\dagger D_3^\dagger|0\rangle.
\end{aligned}
\tag{115}
$$

By identifying an exciton on transmission lines 1 and 3 to correspond to a Boolean 0 and an exciton on transmission lines 2 and 4 to correspond to a Boolean 1, the scattering matrix corresponding to the basis transformation Eq. (115) is given by

$$
\begin{bmatrix}
-1 & 0 & 0 & 0\\
0 & 1 & 0 & 0\\
0 & 0 & 0 & -i\\
0 & 0 & -i & 0
\end{bmatrix}.
\tag{116}
$$

Comparing this with Eq. (20) one sees that this transformation is not quite the standard CNOT gate transformation, but it does exhibit CNOT functionality.

The standard CNOT gate can be obtained from this core by introducing a phase shift of $-\pi/2$ at the transmission line 3 input port and the output port. This is implemented in Fig. 8 by making the transmission line segments for input and output ports 3 one dye shorter than the corresponding transmission line segments for the other input and output ports. That is, one implements the transformations

$$
\begin{aligned}
A_3^{\text{in}\dagger} &= -i A_3^\dagger\\
D_3^\dagger &= -i D_3^{\text{out}\dagger}\\
A_m^{\text{in}\dagger} &= A_m^\dagger \ \text{ if } m \in \{1,2,4\}\\
D_m^\dagger &= D_m^{\text{out}\dagger} \text{ if } m \in \{1,2,4\}\,.
\end{aligned}
\tag{117}
$$

With these equations, Eq. (115) yields

$$\begin{aligned} A_1^{\text{in}\dagger} A_3^{\text{in}\dagger} |0\rangle &= D_1^{\text{out}\dagger} D_3^{\text{out}\dagger} |0\rangle \\ A_1^{\text{in}\dagger} A_4^{\text{in}\dagger} |0\rangle &= D_1^{\text{out}\dagger} D_4^{\text{out}\dagger} |0\rangle \\ A_2^{\text{in}\dagger} A_3^{\text{in}\dagger} |0\rangle &= D_2^{\text{out}\dagger} D_4^{\text{out}\dagger} |0\rangle \\ A_2^{\text{in}\dagger} A_4^{\text{in}\dagger} |0\rangle &= D_2^{\text{out}\dagger} D_3^{\text{out}\dagger} |0\rangle . \end{aligned} \tag{118}$$

The scattering matrix corresponding to this transformation is

$$\begin{bmatrix} 1\,0\,0\,0 \\ 0\,1\,0\,0 \\ 0\,0\,0\,1 \\ 0\,0\,1\,0 \end{bmatrix}, \tag{119}$$

which is the standard scattering matrix, Eq. (20), for the CNOT gate [33].

This completes the demonstration that a set of gates enabling universal quantum computation can be implemented as suitably constructed dye aggregates in which the exciton dynamics is governed by the Frenkel Hamiltonian Eq. (27).

14 Exciton-Based Quantum Computer Architecture

Having discussed individual gates, the overall architecture of an exciton-based quantum computer is presented. Figure 9 indicates what the quantum computer might look like, how it is initialized and how the result of the computation is delivered as output.

Between the two vertical dashed lines is the computer circuit itself. In this case, the circuit for a Fredkin gate was chosen as a stand-in for a general quantum computer circuit [45]. In this case, three qubit lines run parallel to each other from left to right. In the dual-rail representation each of these lines consists of two transmission lines. The boxes represent single qubit gates. The boxes labeled H are Hadamard gates that perform the transformation given by Eq. (17). The boxes labeled T are phase gates performing the transformation

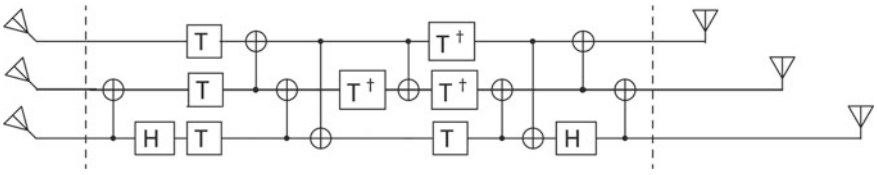

Fig. 9 A schematic indicating the architecture of an exciton-based many-body quantum walk quantum computer. See text for details

$$\begin{bmatrix} 1 & 0 \\ 0 & e^{i\pi/2} \end{bmatrix}.$$

Coupling between qubit wires are through the CNOT gates (Fig. 1).

The input ports are represented by the antennas at the left end of each qubit line. Each of these antennas would couple to a separate electromagnetic field mode. On-demand single photon sources would be coupled to these antennas to generate the exciton input state. In principle the conversion of a photon into an exciton can be done with unit quantum efficiency, but in practice the coupling optics and antenna design could be quite challenging. In addition, the single photon sources would need to emit short optical pulses all timed to simultaneously initiate each qubit. The excitons propagate ballistically (in sync) through the gate network to the output. Note that the number of output lines is the same as the number of input lines. This is a consequence of unitary evolution. The output can be delivered to photodetectors by antennas at the output side (right side of the circuit). These antennas would have the same structure as the input antennas and would, with unit quantum efficiency, convert an exciton to a photon that would then be detected with a unit quantum efficiency photodetector. The output qubit lines (to the right side of the right most vertical dashed line) have been draw to different lengths. Each qubit will thus arrive at its detector at a different time due to propagation delays. In this manner, the output of the quantum computer is time multiplexed so that the output can be read by noting the arrival time of each photon at the photodetector. This scheme has the advantage that only a single photodetector need be employed, which should simplify the optics that delivers the photons to the photodetector.

The quantum computer, as described, is a special purpose device. For each problem to be addressed by quantum computation, a special purpose circuit would be assembled to carry out that computation. In principle, a general purpose quantum computer could be implemented that uses classical switches to reconfigure the circuits. With DNA nanotechnology this might be done using strand displacement techniques to reconfigure the circuit [46].

15 But Isn't a Quantum Computer Just an Analog Computer?

The question posed in this section heading is often expressed. At first sight, constructing a quantum computer is simply a matter of assembling a physical system that implements a desired unitary transformation. Wave interference effects alone enable the implementation of an arbitrary unitary transformation, and this can be done at the classical level with a collection of optical beam splitters [30]. A quantum computer differs in two crucial ways from a classical computer. First, quantum superposition, in effect, enables the same gate to carryout multiple operations simultaneously, which greatly reduces the parts count or the number of steps needed to carry out a computation for those tasks amenable to quantum speedup. Second, if the

gate error rate is below a certain threshold value, quantum error correction can be implemented, enabling scalable quantum computation with imperfect gates [47, 48]. In contrast, the precision and accuracy of analog computers is generally limited by the precision and accuracy of their components. Error correcting quantum computing schemes have been devised for which the tolerance for errors is about 1% per gate operation, which is still quite demanding. Nevertheless, this is a good reach goal to drive technology and the resulting information processing technology is likely to have applications even if full-scale quantum computing is not achieved, particularly because of the compact size (molecular scale) of the gates and the femtosecond switching time for gates employing optical transitions.

16 Molecular Vibrations

A number of imperfections that occur at the molecular level can give rise to gate errors or present challenges that must be overcome to construct viable gates. These include the dispersiveness inherent in exciton transmission lines consisting of an array of dyes, errors in DNA assembly, and Brownian motion that modulates the gate parameters as a function of time. The most serious "imperfections" result from the interaction of excitons with molecular vibrations. How this interaction is modeled is discussed here.

A molecule in its ground state has a structural configuration characterized by the equilibrium position of the nucleus of each atom. Should the molecule absorb a photon and transition to its lowest optically allowed excited state, the position of the atomic nuclei at the instance of the transition will still be in the ground-state equilibrium configuration, as optical transitions occur on a shorter time scale than that required for the atomic nuclei to readjust their positions. As a consequence, the atomic nuclei are displaced from their excited state equilibrium position. The system responds by converting this potential energy into kinetic energy as the nuclei accelerate toward their excited state equilibrium positions. The result is that the molecule undergoes molecular vibrations. These vibrations couple to the environment thereby providing a means of energy exchange between the molecule and the environment. The result is a scrambling of phases that washes out interference effects. This process is referred to as decoherence. This process degrades quantum gate performance, as these gates rely on quantum interference effects.

The exciton–vibration coupling is well modeled by what is often referred to as the Frenkel–Holstein Hamiltonian [49, 50]. This Hamiltonian can be written as the sum of the Frenkel Hamiltonian H_F of Eq. (27) with a Hamiltonian H_V (the Holstein part) characterizing the dynamics of the molecular vibrations and their coupling to the excitons

$$H = H_F + H_V. \tag{120}$$

The Hamiltonian H_V is given by

$$H_V = \sum_{m=1}^{N} \sum_{\alpha} E^v_{m,\alpha} a^\dagger_{m,\alpha} a_{m,\alpha} + \sum_{m=1}^{N} \sum_{\alpha} E^v_{m,\alpha} \lambda_{m,\alpha} B^\dagger_m B_m \left(a_{m,\alpha} + a^\dagger_{m,\alpha}\right) \tag{121}$$

where $a_{m,\alpha}$ is the annihilation operator for a quantum of vibration for the αth vibration mode on molecule m and the Hermitian adjoint $a^\dagger_{m,\alpha}$ is the corresponding creation operator. These satisfy Bose commutation relations similar to those of the excitons Eqs. (33) and (34). $E^v_{m,\alpha}$ is the energy of a quantum of vibration for the αth vibration mode on molecule m, and $\lambda_{m,\alpha}$ is the displacement between the equilibrium position of the ground and excited electronic state for the αth vibration mode on the mth molecule. The sums are over all vibration modes of the molecule and over all molecules.

Some insight into the consequences of the exciton–vibration coupling can be obtained by considering the Heisenberg equation of motion for the exciton annihilation operator B for a single molecule. For a single molecule the full Hamiltonian, neglecting two-exciton terms, becomes

$$H = E^e B^\dagger B + \sum_{\alpha} E^v_\alpha a^\dagger_\alpha a_\alpha + \sum_{\alpha} E^v_\alpha \lambda_\alpha B^\dagger B \left(a_\alpha + a^\dagger_\alpha\right), \tag{122}$$

where, because we are dealing with only one molecule, the molecule index has been suppressed. The Heisenberg equation of motion for B is given by

$$\frac{\mathrm{d}B}{\mathrm{d}t} = \frac{i}{\hbar}[H, B]. \tag{123}$$

For the Hamiltonian Eq. (122) this yields

$$\frac{\mathrm{d}B}{\mathrm{d}t} = -i \left[\omega^e + \sum_{\alpha} \omega^v_\alpha \lambda_\alpha \left(a_\alpha + a^\dagger_\alpha\right)\right] B, \tag{124}$$

where ω^v_α is the vibration frequency of the αth vibration mode and is related to the energy of a quantum of vibration by $E^v_\alpha = \hbar\omega^v_\alpha$. The operator $a_\alpha + a^\dagger_\alpha$ is the position coordinate for the vibrational mode α. Treating this as a classical variable, Eq. (124) can be integrated to yield

$$B(t) = B(0)\mathrm{e}^{-i[\omega^e t + \phi_v(t)]}, \tag{125}$$

where $\phi_v(t)$ is a fluctuating phase arising from the motion of all the molecular vibration modes

$$\phi_v(t) = \int_0^t \sum_{\alpha} \omega^v_\alpha \lambda_\alpha \left(a_\alpha(t') + a^\dagger_\alpha(t)\right) \mathrm{d}t'. \tag{126}$$

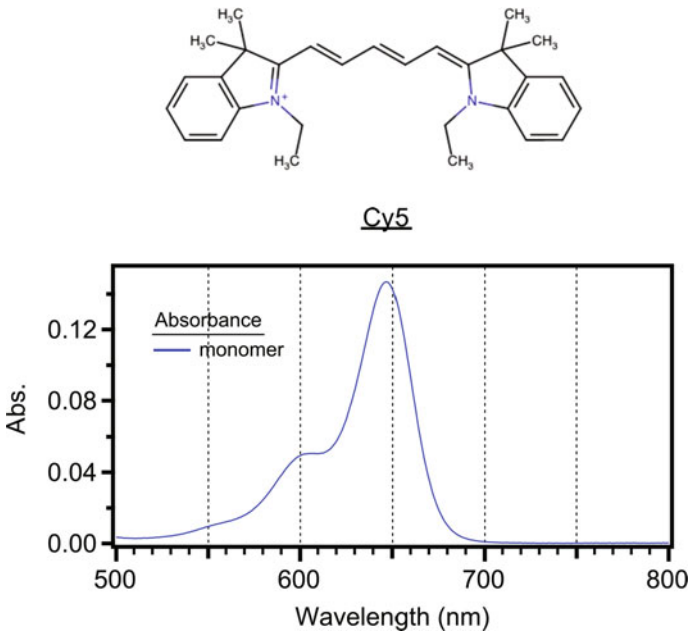

Fig. 10 An example of a dye whose aggregate absorbance and circular dichroism spectra can be well modeled by including only one vibrational mode of the dye. Shown is the cyanine dye Cy5 structure (top panel) and the monomer absorbance spectrum (bottom panel). The shoulder at 600 nm in the absorbance spectrum is due to the dominant vibrational mode. The absorbance units are $10^6\ \mathrm{M}^{-1}\mathrm{cm}^{-1}$

This random phase causes the phase winding of B to deviate from that for pure sinusoidal oscillation $\mathrm{e}^{i\omega^{\epsilon}t}$. This spoils interference effects and gives a width to the spectral lines of the dye absorption and emission spectra.

It is often the case that a coupling between the exciton and vibration is particularly strong for a single or small group of vibration modes [51]. An example of this is the Cyanine dye Cy5 whose structure and absorbance spectrum [42] are shown in Fig. 10. The absorbance spectrum shows an absorbance maximum at about 650 nm. This corresponds to the optical transition from the ground electronic state with no vibrational quanta to the lowest excited electronic state with no vibrational quanta. The shoulder at 600 nm on the short wave-length side of the peak corresponds to the optical transition from the ground electronic state with no vibrational quanta to the lowest excited electronic state with one vibrational quantum for a dominant vibrational mode. In the case when one dominant vibration mode occurs the absorbance spectrum can be well modeled by including only this one vibrational mode for each molecule. In this case the Hamiltonian Eq. (121) reduces to

$$H_V = \sum_{m=1}^{N} E_m^v a_m^\dagger a_m + \sum_{m=1}^{N} E_m^v \lambda_m B_m^\dagger B_m \left(a_m + a_m^\dagger\right). \tag{127}$$

This Hamiltonian is simple enough that the energy eigenstates and eigenvalues can be solved to a high degree of accuracy by numerical methods while still adequately accounting for the spectral features in optical absorption spectra of aggregates.

When an exciton moves from one dye molecule to another, the dye it leaves undergoes a transition from the excited state to the ground state while the dye it moves to undergoes a transition from the ground state to the excited state. Both of these transitions induce molecular vibrations; however, due to conservation of energy the exciton cannot endlessly shed vibrations. As a result, the exciton carries a cloud of vibrations (or molecular distortions) with it [52]. The exciton becomes a composite particle, a bundle of electronic and vibrational energy. This modifies the dispersion relation for an exciton propagating along an exciton transmission line. Nevertheless, it should still be possible to engineer exciton quantum gates that work in spite of the composite nature of the exciton.

It is also noted that molecular vibrations exhibit longer decoherence times than excitons [53]. The exciton hopping interaction provides a means of coupling vibrations between dyes. It is thus an interesting question as to whether quantum computing with dye aggregates could be implemented using quanta of molecular vibrations in which the excitons simply provide a means to control the flow of quantum information from dye molecule to dye molecule.

17 Conclusion

It has been shown that exciton-based quantum gates can be constructed from dye aggregates; and the aggregate configurations for a set of dyes sufficient to enable universal quantum computation have been presented. How these could be assembled into circuits with inputs and outputs has been discussed. In addition, nonidealities resulting from the coupling between excitons and molecular vibrations have been treated.

The question arises: What are the prospects for realizing such devices in practice? Exciton delocalization extending over 30–100 dyes has been reported in the literature [24]. The transmission lines in the largest gate presented, Fig. 8, are 23 dyes long. This suggests that it should be possible to experimentally demonstrate the gates that have been presented, as well as small circuits assembled from such gates. Constructing quantum computers that would be competitive with conventional computers would require that workarounds be devised for a number of nonidealities that dye molecules exhibit.

Although DNA nanotechnology currently offers the most promising means by which to assemble dye aggregates into functioning quantum gates and circuits, the technology still has limitations that make the construction of these gates challenging. It is desirable that the $J_{m,n}$ and $K_{m,n}$ be as large as possible to enable the gate or circuit to complete its operation before coherence is lost. Ideally, the dyes would be stacked as closely as possible. That is, one would like the spacing between dyes to be comparable to the base stacking distance of DNA. The helical twist of DNA, for

which a full turns occurs over roughly 3.4 nm, however, makes it difficult to take advantage of the base stacking to pack dyes closely together. One would like to lay out the gates in a two-dimensional or three-dimensional arrangement. Here the 2 nm diameter of duplex DNA complicates the stacking of dyes close together in the direction orthogonal to the DNA helix direction. The size mismatches between the DNA structure and the desired spacing between dyes could be ameliorated if dyes were covalently linked into transmission-line lengths that could span the distance of a helical turn of DNA or the distance between neighboring duplex strands. Covalently linked aggregates forming gates would also help. DNA assembly would then be used to arrange these larger components into a desired circuit.

Finally, the quantum computer architecture proposed here is not necessarily optimum. Childs et al. [20] provide a different set of gates that could be implemented with dye aggregates in which the exciton–exciton interaction characterized by the anharmonicity parameter Δ_m rather than the exciton–exciton interaction characterized by $K_{m,n}$ provides the exciton–exciton interaction needed to implement controlled basis change gates. A search for alternative means with which to do information processing or quantum computing using dye aggregates could be productive. In this regard, it is noted that molecular vibrations exhibit coherence times that are longer than those of excitons. This suggests that it may be worth considering how molecular vibration quanta might be used to process and store quantum information.

Acknowledgements The author thanks the Boise State University qDNA Device Group for stimulating discussions and is especially appreciative of William B. Knowlton, Joseph Melinger and anonymous reviewers for comments helpful in the preparation of this manuscript. This research was supported wholly by the Department of Navy award No. N00014-19-1-2615 issued by the Office of Naval Research.

Appendix

Here expressions for $J_{m,n}$ and $K_{m,n}$ are presented. Both of these quantities represent Coulomb interaction energies between pairs of dyes. The first results from the Coulomb interaction between the transition charge densities of a pair of dyes, whereas the latter arises from differences in the Coulomb interaction between a pair of dyes resulting from differences in the ground-state and excited-state charge densities of the dyes [34]. Expressions for these energies greatly simplify when the distance between the dye molecules is much greater than the size of the molecule. In this case an approximation can be made in which the charge distribution on a dye is represented by a dipole moment. Even when the distance between the dyes is less than their lengths, the dipole approximation often provides a factor of two estimate for $J_{m,n}$ and $K_{m,n}$.

Consider first $J_{m,n}$. The dipole component of the transition charge density is referred to as the transition dipole. It is a vector quantity whose magnitude for dye m is here denoted by μ_m. The dipole vector generally is parallel to the long axis of

the dye molecule. In the dipole approximation $J_{m,n}$ is given by

$$J_{m,n} = \frac{\mu_m \mu_n}{4\pi\epsilon\epsilon_0 R_{m,n}^3} \left[\cos(\theta_1) - 3\cos(\theta_2)\cos(\theta_3)\right], \tag{128}$$

where $R_{m,n}$ is the distance between the centers of the two dyes, ϵ_0 is the permittivity of free space and ϵ is the relative dielectric constant of the medium in which the dyes reside. θ_1 is the angle the two dyes make with respect to each other, θ_2 is the angle between dye m and the line between the centers of the two dyes. Similarly, θ_3 is the angle between dye n and the line between the centers of the two dyes. Thus four quantities $R_{m,n}$, θ_1, θ_2 and θ_3 that can be adjusted to fine-tune $J_{m,n}$ to a desired value.

Consider now $K_{m,n}$. Let Δd_m denote the magnitude of the dipole component of the difference between the excited-state and ground-state charge densities of molecule m. The direction of this dipole also generally lies along the long axis of the dye molecule. But if the dye molecule has a bent shape or has a width comparable to its length then it need not lie along the long axis of the molecule. It could even be perpendicular to the transition dipole. In general it will have some fixed angle with respect to the transition dipole. In the dipole–dipole approximation one has

$$K_{m,n} = \frac{\Delta d_m \Delta d_n}{4\pi\epsilon\epsilon_0 R_{m,n}^3} \left[\cos(\phi_1) - 3\cos(\phi_2)\cos(\phi_3)\right], \tag{129}$$

As in the case for $J_{m,n}$, four quantities can be varied by adjusting the position or orientation of the two dyes. These are $R_{m,n}$, ϕ_1, ϕ_2 and ϕ_3. Because $R_{m,n}$ is present in both Eqs. (128) and (129) and the transition dipole and the difference static dipole make a fixed angle with respect to each other, the degree to which $J_{m,n}$ and $K_{m,n}$ can be adjusted independently is constrained. When the transition dipoles and difference static dipoles are not parallel, however, $J_{m,n}$ and $K_{m,n}$ can still be adjusted independently of each other over a range of values.

General expressions for $J_{m,n}$ and $K_{m,n}$ are given in [34]; however, their evaluation requires that one obtain the transition and ground-state and excited state-static charge densities for the molecules by an ab initio calculation, such as through density functional theory and time-dependent density functional theory.

References

1. B.H. Robinson, N.C. Seeman, The design of a biochip: a self-assembling molecular-scale memory device. Protein Eng. **1**, 295–300 (1987)
2. X. Yan, S. Huang, Y. Wang, Y. Tang, Y. Tian, Bottom-up self-assembly based on DNA nanotechnology. Nanomaterials **10**, 2047 (2020)
3. Y. Chen, W. Sun, C. Yang, Z. Zhu, Scaling up DNA self-assembly. ACS Appl. Bio Mater. **3**, 2805–2815 (2020)

4. M. Massey, I.L. Medintz, M.G. Ancona, W.R. Algar, Time-gated FRET and DNA-based photonic molecular logic gates AND. OR, NAND, and NOR, ACS Sens. **2**, 1205–1214 (2017)
5. X. Lan, Q. Wang, DNA-programmed self-assembly of photonic nanoarchitectsures. NPG Asia Materials **6**, e97 (2014)
6. Buckhout-White S. Spillmann C.M., Algar W,R., Khachatrian A., Melinger J.S. Goldman E.R., Ancona M.G., Medintz I.: Assembling programmable FRET-based photonic networks using designer DNA scaffolds, Nature Com. **5**, 5615 (2014)
7. Z.-G. Wang, C. Song, B. Ding, Functinal DNA nanostructures for photonic and biomedical applications. Small **9**, 2210–2222 (2013)
8. B. Albinsson, J.K. Hannestad, K. Börjensson, Functionalized DNA nanostructures for light harvesting and charge separation. Coordination Che. Rev. **256**, 2399–2413 (2012)
9. S. Su, V. Bonnard, G.A. Burley, DNA-templated photonic arrays and assemblies: Design principles and future opportunities. Chem. Eur. J. **17**, 7982–7991 (2011)
10. J.S. Huff, D.B. Turner, O.A. Mass, L.K. Patten, C.K. Wilson, S.K. Roy, M.S. Barclay, B. Yurke, W.B. Knowlton, P.H. Davis, R.D. Pensack, Excited-state lifetimes of DNA-templated cyanine dimer, trimer, and tetramer aggregates: The role of exciton delocalization, dye separation, and DNA heterogeneity. J. Phys. Chem. B **125**, 10240–10259 (2021)
11. O.A. Mass, C.K. Wilson, S.K. Roy, M.S. Barclay, L.K. Patten, E.A. Terpetschnig, J. Lee, R.D. Pensack, B. Yurke, W.B. Knowlton, Exciton delocalization in indolenine squaraine aggregates templated by DNA Holliday junction scaffolds. J. Phys. Chem. B **124**, 9636–9647 (2020)
12. Rukin P.S., Komarova K.G., Fresch B., Collini E., Remacle F.: Chirality of a rhodamine heterodimer linked to a DNA scaffold: an experimental and computational study, Phys. Chem. Chem. Phys. textbf22, 7516-7523 (2020)
13. S. Mandal, X. Zhou, S. Lin, H. Yan, N. Woodbury, Directed energy transfer through DNA-templated J-aggregates. Bioconjugate Chem. **30**, 1870–1879 (2019)
14. B.L. Cannon, L.K. Patten, D.L. Kellis, P.H. Davis, J. Lee, E. Graugnard, B. Yurke, W.B. Knowlton, Large Davydov splitting and strong fluorescence suppression: An investigation of exciton delocalization in DNA-templated Holliday junction dye aggregates. J. Phys. Chem. A **122**, 2086–2095 (2018)
15. B.L. Cannon, D.L. Kellis, L.K. Patten, P.H. Davis, J. Lee, E. Graugnard, B. Yurke, W.B. Knowlton, Coherent exciton delocalization in a two-state DNA-templated dye aggregate system. J. Phys. Chem. A **121**, 6905–6916 (2017)
16. H. Asanuma, T. Fujii, T. Kato, H. Kashida, Coherent interactions of dyes assembled on DNA. J. Photochem. Phtobio. C: Photochem. Rev. **13**, 124–135 (2012)
17. M. Wang, G.L. Silva, B.A. Armitage, DNA-templated formation of a helical cyanine dye J-aggregaate. J. Am. Chem. Soc. **122**, 9977–9986 (2000)
18. M.A. Castellanos, A. Dodin, A.P. Willard, On the design of molecular excitonic circuits for quantum computing: the universal quantum gates. Phys. Chem. Chem. Phys. **22**, 3048–3057 (2020)
19. M.A. Castallanos, A.P. Willard, Designing excitonic circuits for the Deutsch-Jozsa algorithm: mitigating fidelity loss by merging gate operations. Phys. Chem. Chem. Phys. **23**, 15196–15208 (2021)
20. A.M. Childs, D. Gosset, Z. Webb, Universal computation by multiparticle quantum walk. Science **339**, 791–794 (2013)
21. M. Kjaergaard, M.E. Schwartz, J. Braumüller, P. Krantz, J.I.-J. Wang, S. Gustavsson, W.D. Oliver, Superconducting qubtis: Current state of play. Annu. Rev. Condens. Matter Phys. **11**, 369–395 (2020)
22. L. Gyongyosi, S. Imre, A survey on quantum computing technology. Comp. Sci. Rev. **31**, 51–71 (2019)
23. J.N. Eckstein, J. Levy, Materials issues for quantum computation. MRS Bulletin **38**, 783–789 (2013)
24. F. Würthner, T.E. Kaiser, C.R. Saha-Möller, J-aggregates: From serendipitous discovery to supramolecular engineering of functional dye materials. Angew. Chem. Int. Ed. **50**, 3376–3410 (2011)

25. Y. Frenkel, On the transformation of light into heat in solids. Phys. Rev. **37**, 17–44 (1931)
26. E.E. Jelley, Spectral absorption and fluorescence of dyes in the molecular state. Nature **138**, 1009–1010 (1936)
27. G. Scheibe, L. Kandler, H. Ecker, Polymerisation and polymere adsorption as a cause of novel absorption bands of organic pigments. Naturwissenschaften **25**, 75–75 (1937)
28. G. Scheibe, A. Mareis, H. Ecker, The reversible polymerisation as a cause of unusual absorption bands III. Naturwissenschaften **25**, 474–475 (1937)
29. G. Scheibe, Über die Veränderlichkeit der Absorptionsspektren in Lösungen und die Nebenvalenzen als ihre Ursache. Angew. Chem. **50**, 212–219 (1937)
30. M. Reck, A. Zeilinger, H.J. Bernstein, P. Bertani, Experimental realization of any discrete unitary operator. Phy. Rev. Lett. **73**, 58–61 (1994)
31. P.W. Shor, Polynomial-time algorithms for prime factorization and discrete logarithms on a quantum computer. SIAM J. Comput. **26**, 1484–1509 (1997)
32. Grover L.K.: A fast quantum mechanical algorithm for database search, Proceedings, 28th Annual ACM Symposium of the Theory of Computing (May 1996), 212-219 (1996)
33. C.P. Williams, *Explorations in Quantum Computing* (Springer, London, 2011), pp.51–122
34. D. Abramavicius, B. Palmieri, S. Mukamel, Extracting single and two-exciton couplings in photosynthetic complexes by coherent two-dimensional electronic spectra. Chem. Phys. **357**, 79–84 (2009)
35. T. Renger, V. May, V. Sudström, O. Kühn, Anharmonic oscillator approach to the exciton-exciton annihilation dynamics in molecular aggregates. J. Chinese Che. Soc. **47**, 807–819 (2000)
36. Jacquemin D.: Excited-state dipole and quadrupole moments: TD-DFT vers CC2, **12** 3993-4003 (2016)
37. G. Barcenas, A. Biaggne, O.A. Mass, C.K. Wilson, O.M. Obukhova, O.S. Kolosova, A.L. Tatarets, E. Terpetschnig, R.D. Pensack, J. Lee, W.B. Knowlton, B. Yurke, LI L: First-principles studies of substituent effects on squaraine dyes. RSC Adv. **11**, 19029–19040 (2021)
38. A. Biaggne, W.B. Knowlton, B. Yurke, J. Lee, L. Li, Substituent effects on the solubility and electronic properties of the cyanine dye Cy5: Density Functional and Time-Dependent Density Functional Theory calaclations. Molecules **26**, 524 (2021)
39. M. Kasha, H.R. Rawls, A. El-Bayoumi, The exciton model in molecular spectroscopy. Pure Appl. Chem. **11**, 371–392 (1965)
40. C. Zhong, D. Bialas, C.J. Collison, F.C. Spano, Davydov splitting in squaraine dimers. J. Phys. Chem. C **123**, 18734–18745 (2019)
41. P.D. Cunningham, S.A. Dí, B. Yurke, I.L. Medintz, J.S. Melinger, Delocalized two-exciton states in DNA scaffolded cyanine dimers. J. Phys. Chem. B **124**, 8042–8049 (2020)
42. M.S. Barclay, S.K. Roy, J.S. Huff, O.A. Mass, D.B. Turner, C.K. Wilson, D.L. Kellis, E.A. Terpetshnig, J. Lee, P.H. Davis, B. Yurke, W.B. Knowlton, R.D. Pensack, Rotaxane rings promote oblique packing and extended lifetimes in DNA-templated molecular dye aggregates. Commun. Chem. **4**, 19 (2021)
43. B. Yurke, W. Kuang, Passive linear nanoscale optical and molecular electronics device synthesis from nanoparticles. Phy. Rev. A **81**, 033814 (2010)
44. K.W. Eccleston, S.H.M. Ong, Compact planar microstripline branch-line and rat-race couplers. IEEE Trans. Microwave Theory Tech. **51**, 2119–2125 (2003)
45. T.S. Humble, H. Thapliyal, E. Muñoz-Coreas, F.A. Mohiyaddin, R.S. Bennink, Quantum computing circuits and devices. IEEE Design & Test **36**, 69–94 (2019)
46. F.C. Simmel, B. Yurke, H.R. Singh, Principles and applications of nucleic acid strand displacement reactions. Chem. Rev. **119**, 6326–6369 (2019)
47. A.M. Stephens, Fault-tolereant thresholds for quantum error correction with the surface code. Phys. Rev. A **89**, 022321 (2014)
48. A.G. Fowler, Surface codes: Towards practical large-scale quantum computation. Phys. Rev. A **86**, 032324 (2012)
49. Barford W., Marcus M.: Theory of optical transitions in conjugated polymers. I. Ideal systems, J. Chem. Phys. **141**, 164101 (2014)

50. W. Barford, O.R. Tozer, Theory of exciton transfer and diffusion in conjugated polymers. J. Chem. Phys. **141**, 164103 (2014)
51. H. Mustroph, A. Towns, Fine structure in electronic spectra of cyanine dyes: Are sub-bands largely determined by a dominant vibration or a collection of singly excited vibrations? Chem. Phys. Chem. **19**, 1016–1023 (2018)
52. F.C. Spano, The spectral signatures of Frenkel polarons in H- and J- aggregates. Accounts of Chem. Res. **43**, 429–439 (2010)
53. J. Lim, D. Paleček, F. Caycedo-Soler, C.N. Lincoln, J. Prior, H. von Berlepsch, S.F. Huelga, M.B. Plenio, D. Zigmantas, J. Hauer, Vibronic origin of long-lived coherence in an artificial molecular light harveter. Nat. Commun. **6**, 7755 (2015)